LIMNOLOGY and OCEANOGRAPHY

Carbon and nutrient cycling in Antarctic landfast sea ice from winter to summer

Elizabeth M. Jones [1,2*,a] Sian F. Henley [3] Maria A. van Leeuwe [4] Jacqueline Stefels [4]
Michael P. Meredith [5] Mairi Fenton, [5,6] Hugh J. Venables [5]

[1] Centre for Energy and Environmental Sciences, University of Groningen, Groningen, The Netherlands
[2] Department of Ocean Systems, NIOZ Royal Netherlands Institute for Sea Research, Utrecht University, Texel, The Netherlands
[3] School of GeoSciences, University of Edinburgh, Edinburgh, UK
[4] Groningen Institute of Evolutionary Life Sciences, University of Groningen, Groningen, The Netherlands
[5] British Antarctic Survey, Cambridge, UK
[6] The Lyell Centre for Earth and Marine Science and Technology, Heriot-Watt University, Edinburgh, UK

Abstract

Seasonal cycling in carbon, alkalinity, and nutrients in landfast sea ice in Hangar Cove, Adelaide Island, West Antarctic Peninsula, were investigated during winter, spring, and summer 2014–2015. Temporal dynamics were driven by changes in the sea-ice physicochemical conditions, ice-algal community composition, and organic matter production. Winter sea ice was enriched with dissolved inorganic carbon (DIC) and inorganic nutrients from organic matter remineralization. Variations in alkalinity (Alk) and DIC indicated that abiotic calcium carbonate (ikaite) precipitation had taken place. Relative to other nutrients, low phosphate (PO_4) concentrations potentially resulted from co-precipitation with ikaite. Seawater flooding and meltwater induced variability in the physical and biogeochemical properties in the upper ice in spring where nutrient resupply supported haptophyte productivity and increased particulate organic carbon (POC) in the interstitial layer. Rapid nitrate (NO_3) and DIC ($< 165\ \mu mol\ kg^{-1}$) uptake occurred alongside substantial build-up of algal biomass (746 μg chlorophyll a L^{-1}) and POC (6191 $\mu mol\ L^{-1}$) during summer. Silicic acid drawdown followed NO_3 depletion by approximately 1 month with a shift to diatom-dominated communities. Accumulation of PO_4 in the lower ice layers in summer likely resulted from PO_4 released during ikaite dissolution in the presence of biofilms. Increased Alk : DIC ratios in the lower ice and under-ice water suggested that ikaite dissolution buffered against meltwater dilution and enhanced the potential for atmospheric CO_2 uptake. This study revealed strong seasonality in carbon and nutrient cycling in landfast sea ice and showed the importance of sea ice in biogeochemical cycling in seasonally ice-covered waters around Antarctica.

*Correspondence: elizabeth.jones@hi.no

Additional Supporting Information may be found in the online version of this article.

[a] Present address: Institute of Marine Research, Fram Centre, Tromsø, Norway

[Correction added on 30 November, 2022, after first online publication: The word ice-sea has been changed to sea-ice throughout the article.]

Sea ice plays an important role in marine productivity and biogeochemical cycling in the seasonally ice-covered ocean around Antarctica (Ducklow et al. 2013; Vancoppenolle et al. 2013; Arrigo 2014). The ice environment is highly dynamic and hosts sympagic (ice-associated) microalgal communities that account for up to 25% of the total primary production in the Southern Ocean (Legendre et al. 1992; Arrigo and Thomas 2004; Saenz and Arrigo 2014). Investigations into cycling of carbon and nutrients in sea ice and air-ice-ocean carbon dioxide (CO_2) exchange have revealed sea ice to be a highly variable and complex biogeochemical component of the Antarctic marine environment (Gleitz et al. 1995; Rysgaard et al. 2007; Fripiat et al. 2017). Two major sea-ice types can be discerned—landfast ice and pack ice. Whereas pack ice is free drifting sea ice, which moves with winds and currents, landfast sea ice is attached to the coast, shallow seafloor or grounded icebergs (Fraser et al. 2020). Landfast ice usually forms and dissipates seasonally, controlled by

atmospheric and oceanic conditions and creates a unique environment due to snow accumulation that regulates exchange of heat and CO_2 between the atmosphere and ocean (Murphy et al. 1995). Sea ice is important as a habitat for sympagic (ice-associated) organisms, including microorganisms and zooplankton (Arrigo et al. 1995; Günther and Dieckmann 1999; Thomas and Dieckmann 2010).

Sea ice is permeated by channels and pores that are filled with brine and enable biogeochemical exchanges, for example, CO_2 and oxygen, between the air and the ocean and allow colonization by microorganisms including sea-ice algae, bacteria, and viruses (Thomas and Dieckmann 2010; van Leeuwe et al. 2018). Sea-ice algae usually begin to grow earlier in the season than phytoplankton in surface waters, likely due to more stable light levels compared with the upper ocean (van Leeuwe et al. 2022). The winter stocks of nutrients trapped within brine pockets fuel springtime production and can be replenished through intense recycling and remineralization in the ice, seawater flooding, ice-ocean exchanges and redistribution of inorganic carbon and nutrients within the ice matrix through freeze thaw cycles (Henley et al. 2012; Vancoppenolle et al. 2013; Fripiat et al. 2017). As ice-algal primary production is largely dominated by diatoms (Thomas and Dieckmann 2010), silicic acid could become limiting during the growing season (Fripiat et al. 2017). Sympagic algal communities are ubiquitous in Antarctic sea ice and have potential to seed pelagic phytoplankton blooms (van Leeuwe et al. 2022). They furthermore contribute to enhanced overall primary production in the sea-ice zone of coastal Antarctica (Smith and Nelson 1985; Vernet et al. 2008; van Leeuwe et al. 2020).

Sea-ice carbon and nutrient dynamics are controlled by physical conditions (Perovich et al. 2004; Nomura et al. 2010), exchanges across air-ice-ocean interfaces (Jones and Coote 1981; Delille et al. 2007; Miller et al. 2011) and biotic processes that cycle carbon and nutrients between the inorganic and organic reservoirs (Legendre et al. 1992; Gleitz et al. 1995; Kennedy et al. 2002). The carbonate system is also affected by abiotic calcium carbonate (ikaite, $CaCO_3 \cdot 6H_2O$) formation and dissolution (Jones and Coote 1981; Rysgaard et al. 2007; Dieckmann et al. 2008). Respiration and remineralization of organic matter by the winter ice-algal community increases the dissolved inorganic carbon (DIC) and nutrient concentrations in the brine (Miller et al. 2011). As sea ice forms, precipitation of ikaite leads to a partitioning of alkalinity (as ikaite crystals) in the ice and DIC (as dissolved CO_2) in the brine (Rysgaard et al. 2007; Dieckmann et al. 2008). Typically, brine is rejected from the growing sea ice into the underlying seawater, whilst some remains trapped in the pockets and channels of the ice. (Jones and Coote 1981; Fransson et al. 2011, 2013). The ikaite crystals are retained within the ice matrix (Rysgaard et al. 2007). Dissolution of ikaite during ice melt increases alkalinity in the meltwater that slightly counteracts dilution effects and promotes drawdown of atmospheric CO_2 in Antarctic coastal waters (Hauri et al. 2015;

Jones et al. 2017; Legge et al. 2017). The CO_2 released during ikaite precipitation and subsequently transported from the ice could be exported below the mixed layer with the saline brine, thus constituting a sea-ice carbon pump (Rysgaard et al. 2007; Fransson et al. 2011). Alongside processes associated with the seasonal formation and melt of sea ice, the sea-ice-driven CO_2 pump makes a small yet significant contribution (Moreau et al. 2015) to the marine carbon cycle of coastal Antarctica (Delille et al. 2014; Legge et al. 2015; van der Linden et al. 2020).

The West Antarctic Peninsula shelf is an ecologically important region that supports high rates of primary production and concomitant substantial biological carbon uptake (Ducklow et al. 2007; Clarke et al. 2008; Brown et al. 2019). These processes drive strong seasonal sinks for atmospheric CO_2 in the coastal zone (Arrigo et al. 2008; Legge et al. 2015; Jones et al. 2017; Brown et al. 2019). Winter pack ice along the West Antarctic Peninsula provides food sources for juvenile krill and is a key regulator of krill recruitment, which is critical for ecosystem productivity and trophic coupling in the Peninsula region and downstream in the Scotia Sea (Saba et al. 2014). Ongoing changes in the sea-ice and marine environment of the West Antarctic Peninsula may have implications for local and regional-scale ice-ocean physical processes, primary production, biogeochemical cycling, and climate (Schofield et al. 2010; Ducklow et al. 2013; Henley et al. 2019).

Previous studies in Antarctic sea ice have documented aspects of seasonal carbon and nutrient dynamics and their linkage to physical processes and ice-algal biodiversity and productivity (Fransson et al. 2011; Henley et al. 2012; Fripiat et al. 2017; Torstensson et al. 2018; van der Linden et al. 2020). However, the key controls of sea-ice inorganic carbon chemistry coupled to physical–chemical–biological processes across different seasons remain largely unresolved. The major aim of this study was to characterize the changes in inorganic carbon and nutrients in Antarctic landfast sea ice in relation to the physicochemical environment and ice-agal community during the seasonal transitions from winter to spring to summer. The main hypotheses were that seasonality in abiotic and biotic processes in landfast sea ice would significantly impact (i) carbon and nutrient cycling from the period of ice formation in autumn/winter to ice melt in spring/ summer and (ii) ice-ocean exchanges and potential for atmospheric CO_2 uptake during summer sea-ice melt.

Due to the remoteness of the sea-ice–covered areas in coastal Antarctica, much of this region remains undersampled and there is a lack of seasonal studies investigating carbon cycling in sea ice. The British Antarctic Survey at Rothera Research Station, West Antarctic Peninsula, carries out year-round marine monitoring in Ryder Bay for the Rothera Oceanographic and Biological Time Series (RaTS), which was initiated in 1997 (Clarke et al. 2008; Venables et al. 2013). Ryder Bay and several smaller embayments in the vicinity (Fig. 1) are
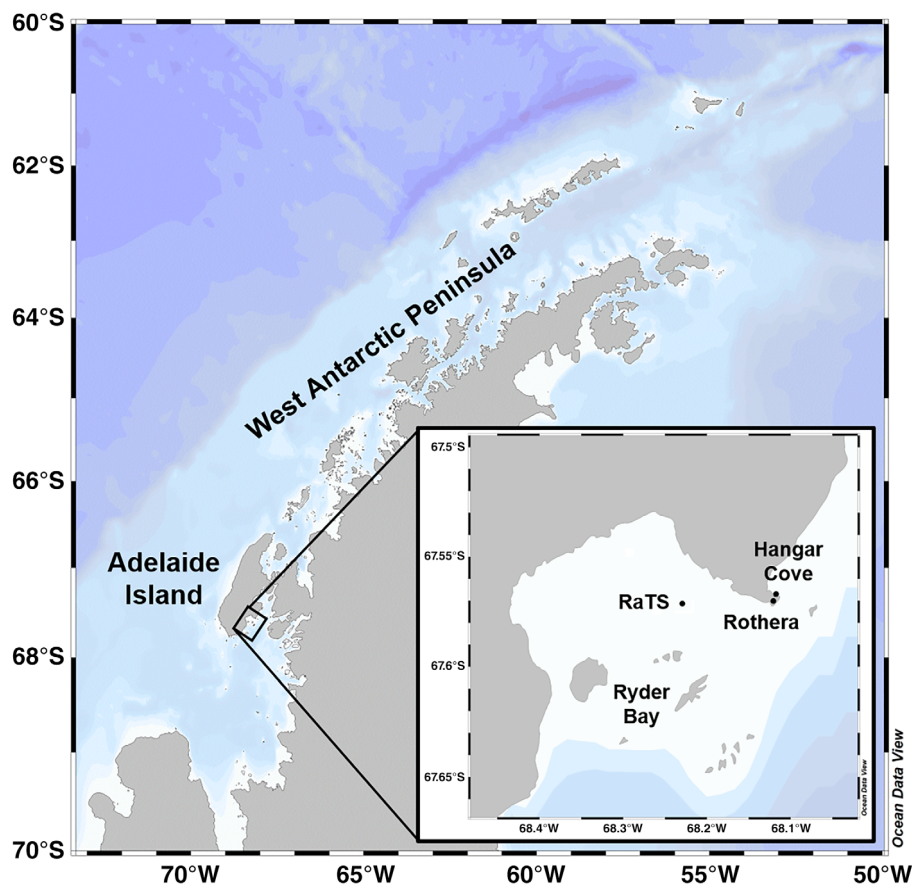
Fig. 1. Map of the West Antarctic Peninsula showing Adelaide Island and (insert) the location of Ryder Bay, Hangar Cove, Rothera Research Station, and the RaTS site. Maps were created with Ocean Data View 4 (http://odv.awi.de; Schlitzer 2018).

located within the seasonally ice-covered coastal zone and are usually covered in landfast ice from June to October, with variable or no ice cover from November/December to March/May (Meredith et al. 2008). This area is ideally suited to conduct a temporal study to address key knowledge gaps in carbon and nutrient cycling in Antarctic landfast sea ice. This study presents new data during winter, spring, and summer from landfast sea ice of the West Antarctic Peninsula to add to the understanding of the intricate linkages between biogeochemical processes, shifts in sympagic microorganisms and ice-ocean exchanges, and further highlights the importance of inorganic carbon cycling in sea ice in the context of potential impacts on the ice-ocean CO_2 system in a scenario of diminishing seasonal sea ice.

Methods

Sea-ice sampling

Seasonal sampling of landfast sea ice was carried out in two phases, during austral winter, spring, and summer 2014 and during winter 2015 (Table 1) in Hangar Cove (67.564°S, 68.130°W), adjacent to Ryder Bay on Adelaide Island, West

Antarctic Peninsula (Fig. 1). Ice cores were taken for biogeochemical analyses (carbonate chemistry, inorganic nutrients, organic matter, stable oxygen isotopes of water), biological variables (photosynthetic pigments and community composition) and physical measurements (temperature, salinity) during 15 sampling events (Table 2). All ice cores were taken within 1–2 d during each sampling event using a 0.09-m–diameter ice corer (Kovacs) from within ~ 1 m^2 area of landfast sea ice in Hangar Cove and are used to form a pseudo-time series, that is, winter–spring 2015 and spring–summer 2014. It is assumed that the physicochemical conditions in the sea ice sampled in winter and early spring 2015 are representative of winter conditions prior to the growing season and period of ice melt. Previous studies have reported strong seasonality for some seasons in aspects of biogeochemical cycling relative to year-to-year variability in sea ice of coastal Antarctica (Henley et al. 2012; Fripiat et al. 2017; van der Linden et al. 2020). Therefore, this study will utilize the physical and biogeochemical changes in the landfast sea ice between winter–spring 2015 and spring–summer 2014 with the biological patterns from winter to summer 2014 to characterize the seasonality in a conceptual model, inferring seasonal changes in landfast sea ice of the West

Table 1. Seasonal sampling for landfast sea-ice and under-ice water in Hangar Cove (67.564°S, 68.130°W) and ice-free seawater in Ryder Bay (67.570°S, 68.225°W). Physical (temperature and salinity), biogeochemical (carbonate chemistry, inorganic nutrients, organic matter, stable oxygen isotopes), and biological (photosynthetic pigments and community composition) properties in ice cores. — indicates no data.

	Physical	**Biogeochemical**	**Biological**
Sea ice	Winter (Jul–Aug 2015)	Winter (Jul–Aug 2015)	Winter (Aug 2014)
	Early spring (Sep–Oct 2015)	Early spring (Sep–Oct 2015)	Early spring (Sep–Oct 2014)
	Late spring (Nov 2014)	Late spring (Nov 2014)	Late spring (Nov 2014)
	Summer (Dec 2014)	Summer (Dec 2014)	Summer (Dec 2014)
Under-ice water	Summer (Dec 2014)	Summer (Dec 2014)	—
Seawater	Autumn (Mar–May 2015)	Autumn (Mar–May 2015)	—
	Winter (Jun–Jul 2015)	Winter (Jun–Jul 2015)	—
	Early spring (Sep–Oct 2015)	Early spring (Sep–Oct 2015)	—
	Late spring (Nov 2014)	Late spring (Nov 2014)	—
	Summer (Dec 2014)	Summer (Dec 2014)	—

Antarctic Peninsula. Samples for bulk sea-ice carbonate chemistry, macronutrient, and particulate organic matter concentrations, stable oxygen isotopes, and salinity were taken and processed following the procedures outlined below. Snow cover and slush layers, such as that observed in late October and early November 2014, were excluded from biological and chemical analyses but are included in descriptions of the ice environment and discussions of seasonal processes.

Physical measurements

The thickness of the landfast sea ice was inferred from the length of each ice core (Table 2), referred to as sea-ice thickness hereafter. The total sea-ice thickness was used as an absolute value (100%) to determine the relative depth of the physical, biogeochemical and biological measurements vertically in each ice core. Due to the seasonal variations in ice thickness and for relevant comparisons of physical and biogeochemical properties at different depth intervals, such as at the air-ice and sea-ice interfaces, relative ice core depths (%) were determined. Vertical gradients in physicochemical properties within the ice (Fig. 2) were used to discriminate key layers (at the specified range of relative ice core depth): upper ice (0–20%), interior ice (20–80%), lower ice (80–100%), air-ice interface (0–10%), and sea-ice interface (90–100%). Vertical patterns in sea-ice properties have been previously used to identify different layers (using relative depths) within landfast ice (van der Linden et al. 2020) and pack ice (Fripiat et al. 2017; Torstensson et al. 2018) around Antarctica.

Sea-ice temperature was measured immediately after core extraction using a calibrated temperature probe (accuracy ± 0.2°C; TESTO 720) inserted into predrilled holes (5–10 cm intervals) along the length of the ice core. Due to logistical constraints, it was not possible to obtain temperature measurements during spring and summer. Salinity (absolute; g kg^{-1}) of the ice melt from the carbonate chemistry and nutrients cores and the under-ice water was measured using a conductivity meter (accuracy ± 0.1 mS cm^{-1}; TPS WP-84). The meter was calibrated with a standard reference conductivity solution (KCl) in addition to a dilution series using MilliQ water and Certified Reference Material of known salinity, which was also used for carbonate chemistry analyses (details below). Brine volume was determined from temperature and salinity measurements following Cox and Weeks (1983).

Biogeochemical coring and analyses

The biogeochemical ice cores comprise two core sets: (1) carbonate chemistry and nutrients (with salinity measurements and the stable oxygen isotopes) and (2) nutrients and organic matter. The carbonate chemistry and nutrients ice cores (winter–early spring 2015 and spring–summer 2014; total 13 cores; Table 2) were cut into 0.05–0.15 m sections using a stainless-steel saw and placed in plastic bags, which were sealed and stored in an insulated cool box for transportation to the laboratory. Core section lengths were dependent on proximity to the ice-water interface, with the bottom-ice section usually being 0.05–0.10 m in length. Core sections for carbonate chemistry analysis were transferred immediately to 1-liter gas-tight Tedlar bags and vacuum-sealed using a Nalgene hand pump and left to melt in the dark at ambient temperature (20°C). Upon complete melt (∼ 20 h), subsamples for DIC and total alkalinity were transferred to 250-mL borosilicate glass bottles, poisoned with 50 μL saturated mercuric chloride solution and stored in the dark until analysis. Seawater and bulk ice analysis for DIC and alkalinity was carried out using a VINDTA 3C (Versatile INstrument for the Determination of Total Alkalinity) in the laboratory at Rothera, following Dickson et al. (2007). Determination of DIC was made by sample acidification with 8.5% H_3PO_4 and gas extraction followed by coulometric analysis (Johnson et al. 1987). The determination of alkalinity was carried out by potentiometric titration with 0.1 M hydrochloric acid (Dickson 1981). The accuracy was checked against Certified Reference Material (CRM, batch

Table 2. Sampling seasons, date (sampling event), and characteristics of landfast sea ice in Hangar Cove (67.564°S, 68.130°W). Biogeochemical and biological data are vertically integrated values from the top (ice-air) to the bottom (sea-ice) of each ice core. The ice-core sets are marked carbonate chemistry and nutrients (total 13 cores), nutrients and organic matter (total 11 cores), biological (total 12 cores). Multiple entries per sampling event indicate the number of different cores taken. — indicates no data.

Core set			Carbonate chemistry and nutrients/nutrients and organic matter				Carbonate chemistry and nutrients		Nutrients and organic matter		Biological			
Season	Date dd mm yy	Ice thickness m	Si(OH)$_4$ mmol m^{-2}	NO$_3$ mmol m^{-2}	NO$_2$ mmol m^{-2}	PO$_4$ mmol m^{-2}	Alkalinity mmol m^{-2}	DIC mmol m^{-2}	POC mmol m^{-2}	PN mmol m^{-2}	Chl a mg m^{-2}	Fuco mg m^{-2}	Hexa mg m^{-2}	Allo mg m^{-2}
Winter	28 Jul 2015*	0.74*	6.90*†‡	2.91*†‡	0.06*†‡	0.18*†‡	234*	234*	—	—	—	—	—	—
Winter	17 Aug 2014	0.36	—	—	—	—	—	—	—	—	0.35	0.08	0.02	0.02
	18 Aug 2015*	0.77*	10.56*†	3.98*†	0.081*	0.19*†	378*	344*	—	—	—	—	—	—
Spring	24 Sep 2014	0.47	—	—	—	—	—	—	—	—	4.79	1.87	0.22	0.54
	25 Sep 2015*	0.93*	10.98*†	4.24*†	0.07*†	0.12*†	414*	388*	—	—	—	—	—	—
Spring	14 Oct 2014	0.58	—	—	—	—	—	−314*	—	—	5.16	2.40	0.03	0.79
	19 Oct 2015*	0.90*	9.06*†	3.75*†	0.04*†	0.23*†	345*	—	—	—	—	—	—	—
Spring	04 Nov 2014	0.75	2.43‡	0.51‡	0.02‡	0.39‡	—	—	58	4	—	—	—	—
	04 Nov 2014	0.62	—	—	—	—	—	—	—	—	3.78	1.89	0.20	0.03
Spring	07 Nov 2014	0.76	3.85‡	1.39‡	0.02‡	0.35‡	—	345	123	13	—	—	—	—
	08 Nov 2014	0.75	3.11†	0.09†	0.00†	0.02†	344	—	—	—	—	—	—	—
Spring	12 Nov 2014	0.74	0.96‡	0.47‡	0.02‡	0.17‡	—	—	60	5	—	—	—	—
	12 Nov 2014	0.76	—	—	—	—	—	—	—	—	9.49	5.42	0.32	0.05
	17 Nov 2014	0.80	2.26‡	0.43‡	0.02‡	0.46‡	—	—	188	18	—	—	—	—
	18 Nov 2014	0.90	4.96†	0.25†	0.01†	0.09†	377	290	—	—	—	—	—	—
	18 Nov 2014	0.83	—	—	—	—	—	—	—	—	4.24	2.40	0.05	0.03
Spring	23 Nov 2014	0.70	2.09‡	0.75‡	0.03‡	0.38‡	—	—	72	5	—	—	—	—
	24 Nov 2014	0.70	3.43†	0.72†	0.01†	0.41†	224	177	—	—	—	—	—	—
	25 Nov 2014	0.87	—	—	—	—	—	—	—	—	8.15	4.23	0.30	0.02
Spring	28 Nov 2014	0.75	3.12‡	0.81‡	0.03‡	0.36‡	—	—	158	11	—	—	—	—
	29 Nov 2014	0.75	2.30†	1.03†	0.01†	0.39†	277	197	—	—	—	—	—	—
	29 Nov 2014	0.75	—	—	—	—	—	—	—	—	6.46	3.21	0.34	0.01
Summer	02 Dec 2014	0.75	2.93‡	2.67‡	0.03‡	0.66‡	—	—	263	21	—	—	—	—
	03 Dec 2014	0.73	2.67†	0.65†	0.02†	0.29†	218	155	—	—	—	—	—	—
	03 Dec 2014	0.73	—	—	—	—	—	—	—	—	19.66	11.00	0.63	0.02
Summer	05 Dec 2014	0.75	3.12‡	0.32‡	0.04‡	0.29‡	—	—	207	13	—	—	—	—
	06 Dec 2014	0.75	1.67†	0.85†	0.01†	0.38†	201	137	—	—	—	—	—	—
	06 Dec 2014	0.70	—	—	—	—	—	—	—	—	15.32	7.90	0.29	0.01
Summer	11 Dec 2014	0.76	2.66‡	0.89‡	0.02‡	0.36‡	—	—	574	41	—	—	—	—
	12 Dec 2014	0.75	1.55†	0.87†	0.01†	0.31†	189	133	—	—	—	—	—	—
	12 Dec 2014	0.71	—	—	—	—	—	—	—	—	29.48	17.14	0.23	0.02
Summer	17 Dec 2014	0.61	0.72‡	0.11‡	0.02‡	0.07‡	—	—	43	4	—	—	—	—
	18 Dec 2014	0.60	0.51†	0.27†	0.00†	0.10†	93	60	—	—	—	—	—	—
	20 Dec 2014	0.60	—	—	—	—	—	—	—	—	66.50	36.69	0.38	0.01
Summer	21 Dec 2014	0.65	1.93‡	0.11‡	0.03‡	0.53‡	—	—	236	18	—	—	—	—
	22 Dec 2014	0.75	1.45†	0.79†	0.02†	0.50†	129	94	—	—	—	—	—	—

*Biogeochemical cores collected in 2015 combined with biological core data from winter–spring–summer 2014 to form a pseudo-time series.
†Data on carbonate chemistry and nutrients.
‡Data on nutrients and organic matter.

130), supplied by A. G. Dickson (Scripps Institute of Oceanography), measured every 10–20 samples. The precision of the DIC and alkalinity measurements was 1.7 and 1.5 μmol kg^{-1}, respectively, based on the average difference between successive duplicate analyses of each CRM bottle ($n = 54$). Subsamples for the analysis of macronutrients were filtered using Acrodisc PF syringe filters (0.2 μm pore size) into prerinsed 5-mL polyethylene vials and stored at 4°C for silicic acid (Si [OH]$_4$) and at -20°C for nitrate plus nitrite (NO$_3$ + NO$_2$) and phosphate (PO$_4$) analyses. Samples were analyzed using a Technicon TrAAcs 800 gas segmented continuous flow analyzer at the Royal Netherlands Institute for Sea Research, Texel. During each run a freshly diluted standard was measured to track instrument performance. Precision for Si(OH)$_4$, PO$_4$, NO$_3$ + NO$_2$, and nitrite (NO$_2$) was determined as 0.27, 0.014, 0.14, and 0.01 μmol L^{-1}, respectively.

Analysis of macronutrients was also conducted separately on cores taken for nutrients and organic matter (spring–summer 2014; total 11 cores; Table 2). Samples were thawed in the dark at 4°C to reduce the risk of algal cell rupture, filtered using Acrodisc PF syringe filters (0.2 μm pore size), and stored in acid-clean high density polyethylene (HDPE) Nalgene bottles at -20°C. Prior to analysis, samples were thawed for 48 h to ensure complete redissolution of silicate precipitates to Si(OH)$_4$ and were analyzed for Si(OH)$_4$, PO$_4$, NO$_3$ + NO$_2$, and NO$_2$ using a Technicon AAII segmented flow autoanalysis system at Plymouth Marine Laboratory, UK. Instrument performance was assessed using CRM from General Environmental Technos Co. Precision for Si(OH)$_4$, PO$_4$, NO$_3$ + NO$_2$, and NO$_2$ was generally better than 0.6, 0.02, 0.2, and 0.01 μmol L^{-1}, respectively. Samples for particulate organic carbon (POC) and particulate nitrogen (PN) were also taken from the nutrients and organic matter core set (spring–summer 2014; Table 2), thawed and filtered through muffle-furnaced 25-mm–diameter GF/F filters (~ 0.7 μm pore size) using a vacuum filtration system. Filters were dried at 50°C overnight, snap frozen at -80°C and stored at -20°C for analysis at the University of Edinburgh. Following Henley et al. (2012), samples were decarbonated prior to analysis by rewetting with Milli-Q water and fuming with 50% HCl for 24 h, and then dried at 50°C overnight. Samples were analyzed for POC and PN using a Carlo Erba NA 2500 elemental analyzer in-line with a VG Prism III Isotope Ratio Mass Spectrometer. The concentrations of POC and PN were calibrated to an acetanilide elemental standard. Following Fripiat et al. (2017), it is assumed that for non-flagellate–dominated communities the contribution of nutrients from algal cell rupture to the NO$_3$, PO$_4$ and Si(OH)$_4$ pools in ice meltwater is minor and would only represent a small fraction of the measured concentrations in the bulk sea ice (within the analytical precision).

Biogeochemical data (X) measured at in situ salinity (sal) were salinity normalized (X_{sal}) to remove effects of concentration and dilution due to salinity changes following the traditional method $X_{\text{sal}} = X/\text{sal} \times 33.4$ (Friis et al. 2003). The relationships among carbon, inorganic nutrients and organic matter, and Chl a were tested for statistical significance (using probability p-values) using linear regression; $p \leq 0.05$ shows that relationship is significant and the two variables are closely coupled and when $p > 0.05$ the relationship is not significant and the two variables exhibit weak or no coupling.

Subsamples for the standardized ratio of stable oxygen isotopes in seawater (δ^{18}O) were taken from the carbonate chemistry and nutrients cores collected on 19 October 2015, 03 December 2014, and 12 December 2014. Ice melts were transferred into 50-mL glass bottles and sealed with stoppers and crimp caps. These were stored in the dark at 4°C until analysis using stable isotope mass spectrometry at the Natural Environment Research Council Isotope Geosciences Laboratory. Data were standardized relative to Vienna Standard Mean Ocean Water for oxygen with a precision better than 0.05‰. Further details on stable oxygen isotope analyses are provided in Meredith et al. (2017).

Biological coring and analyses

The biological ice cores (winter–spring–summer 2014; total 12 cores; Table 2) were cut into ca. 10-cm sections on site, transferred into Nalgene pots and placed into an insulated cool box for transport to the laboratory. Ice sections were melted at 2°C in hypersaline water, under dark conditions, over 24–48 h. Small aliquots (50–500 mL) were filtered gently (< 15 kPa) over a GF/F filter (Whatman), subsequently snap-frozen in liquid nitrogen and stored at -80°C until analysis. Before extraction in 90% acetone, filters were freeze-dried at -55°C over 48 h. Pigments were analyzed by high-performance liquid chromatography on a Waters system equipped with a photodiode array detector (Van Heukelem and Thomas 2001; van Leeuwe et al. 2006). A Zorbax C8, 3.5-μm column was used. Pigment standards were obtained from DHI Water Quality Institute.

Under-ice water and ice-free seawater sampling

Under-ice water was collected during summer (December 2014; Table 1) using a 12-V electric bilge pump attached to silicon tubing with the inlet lowered to ~ 10 cm below the base of the ice.

Seawater sampling in Ryder Bay (RaTS; Fig. 1) was carried out in autumn (March–May 2015), winter (June–July 2015), spring (September–November 2014), and summer (December 2014; Table 1) following procedures described in Jones et al. (2017). Briefly, seawater was collected from 3.5-L Niskin bottles attached to a line equipped with a conductivity, temperature, and depth sensor package (Seabird SBE19+). Samples for carbonate chemistry were drawn into 250-mL borosilicate glass bottles and analyzed as described above. Samples for macronutrients and for the stable oxygen isotope of seawater

were collected and analyzed as described above for the ice core melts.

Scenarios of sea-ice carbonate chemistry dynamics and implications for atmospheric CO_2 uptake in seasonally ice-covered waters

The influence of sea-ice ikaite processes on summer surface waters and atmospheric CO_2 uptake can be examined by considering scenarios where precipitation and dissolution of ikaite in landfast sea ice occurs (where Alk : DIC ~ 1.0) and does not occur (where Alk : DIC ~ 2.3). Summer average values (from data in Table 2) for salinity (4.9), $Si(OH)_4$ (3.4 μmol kg^{-1}), PO_4 (0.7 μmol kg^{-1}), and DIC (200 μmol kg^{-1}) in sea ice and estimated temperature ($-1°C$) and varying Alk : DIC (driven by alkalinity changes) were used to assess the impact of ikaite dissolution on surface seawater during ice melt. The sea-ice meltwater is assumed to completely and conservatively mix into the summer surface layer. In the first scenario, no ikaite precipitation/dissolution takes place in the ice and the Alk : DIC ratio is ~ 1.0, so the sea-ice alkalinity value is adjusted to 205 μmol kg^{-1}. For the second scenario, ikaite precipitation/dissolution takes place and excess alkalinity released results in a Alk : DIC ratio of 2.3. Therefore, the sea-ice alkalinity value is adjusted to 450 μmol kg^{-1}. Summer mixed-layer average (Table 2) salinity (33.2), $Si(OH)_4$ (57.4 μmol kg^{-1}), PO_4 (1.1 μmol kg^{-1}), alkalinity (2267 μmol kg^{-1}), DIC (2061 μmol kg^{-1}), and temperature (0.5°C from Jones et al. 2017) are taken as representative of ice-free seawater in Ryder Bay.

Typical mixed layer depths in ice-free waters during summer were 8 ± 7 m from previous work in Ryder Bay (table 1 in Jones et al. 2017). It is assumed that sea-ice meltwater stratifies the water column to form an approx. 2 m meltwater lens (Jones et al. 2017) capping an approx. 8-m–deep summer mixed layer. Following similar approaches to Rysgaard et al. (2007) and Fransson et al. (2011), the ice meltwater is assumed to mix completely and conservatively with the surface seawater, resulting in a meltwater-influenced mixed layer with salinity 26.1, temperature 0.12°C, $Si(OH)_4$ 43.9 μmol kg^{-1}, PO_4 1.0 μmol kg^{-1}, DIC 1596 μmol kg^{-1}, and alkalinity 1752 (first scenario) and 1813 μmol kg^{-1} (second scenario). These values fall within the ranges actually measured in the under-ice water during summer (Table 2) and are thus considered representative of values in seawater proximal to melting sea ice in this region. The CO_2 speciation program CO2SYS (Pierrot et al. 2006) was used to calculate the partial pressure of CO_2 (pCO_2) in the seawater, following the procedures and using the dissociation constants reported in Fransson et al. (2011).

Results

Sea-ice physical properties

The average thickness of the landfast sea ice in winter (July–August) was 0.62 ± 0.23 m, in spring (September–

November) was 0.75 ± 0.14 m and in summer (December) was 0.70 ± 0.07 m (Table 2). The sea ice present from August to October 2015 was thicker (0.77–0.93 m) compared with the ice in 2014 (0.36–0.58 m) at the same time of year. Ice temperatures were only collected during winter and early spring (October) in 2015 and varied between $-10.3°C$ and $-1.5°C$, from coldest in the upper ice to warmest at the lower ice (Fig. 2a). Depth profiles were more isothermal in spring. Salinity in winter and early spring ice typically exhibited C-shaped profiles and was generally lower in the 20–50% (from ice core top to base) depth range (Fig. 2b). Average sea-ice bulk salinity (i.e., combined ice and brine inclusions) was 6.4 ± 1.6 in winter, 7.2 ± 2.2 in spring, and 4.9 ± 1.6 in summer. Brine volume was lowest (< 5%) in the cold upper part of the winter ice and highest volumes (> 20%) occurred in the warmer ice in October (Fig. 2c). A slush layer had developed in November in the upper 20–30%, as observed during sampling. Despite limited sea-ice $\delta^{18}O$ data available, the large temporal differences in the $\delta^{18}O$ values can be used to infer distinct seasonal processes and signals in the landfast ice. Values of $\delta^{18}O$ in October were low and ranged from $-1.88‰$ at the top of the ice, $-3.21‰$ in the lower part of the ice, and $-1.97‰$ at the base (Fig. 2d). The distribution of sea-ice $\delta^{18}O$ in early December was more variable with values between 1.73‰ in the upper 50% and $-1.16‰$ in the lower 90% of the ice. The upper part of the ice was isotopically heavy as $\delta^{18}O$ was $1.58‰ \pm 0.13‰$ in contrast to the lower 50% of the ice that was relatively isotopically light ($-0.65‰ \pm 0.58‰$). A seawater salinity reference of 33.4 ± 0.3 was determined as an average from the upper layer (0–15 m) in ice-free water in Ryder Bay, west of Hangar Cove (Fig. 1), during the main ice core and under-ice water sampling period (23 July–17 January).

Sea-ice macronutrients

Concentrations of sea-ice $Si(OH)_4$, NO_3, and NO_2 were highest in winter and displayed more homogenous vertical distributions and low concentrations in summer (Fig. 3a–c). Concentrations of $Si(OH)_4$ and NO_3 were high at 29.8 and 11.9 μmol L^{-1}, respectively, in winter compared with very low concentrations < 1.0 μmol L^{-1} in summer. The summer sea-ice $Si(OH)_4$ minimum appeared to lag that of NO_3 by approximately 1 month. Elevated concentrations of $Si(OH)_4$ (17.1 μmol L^{-1}), NO_3 (33.1 μmol L^{-1}), and NO_2 (0.18 μmol L^{-1}) were measured at the sea-ice interface in early December. Concentrations of PO_4 were distinctly low (< 0.60 μmol L^{-1}) and relatively homogenous throughout the ice during winter and spring and increased in the lower ice to a maximum of 6.69 μmol L^{-1} at the ice base in December (Fig. 3d). Depth-integrated NO_3 was lowest (0.09 mmol m^{-2}) in early November and highest (4.40 mmol m^{-2}) in August (Table 2). Similarly, depth-integrated NO_2 was higher (0.06–0.08 mmol m^{-2}) from July to September, after which values remained low (≤ 0.04 mmol m^{-2}). For $Si(OH)_4$, depth-integrated concentrations were lowest (0.51 mmol m^{-2}) in December and highest
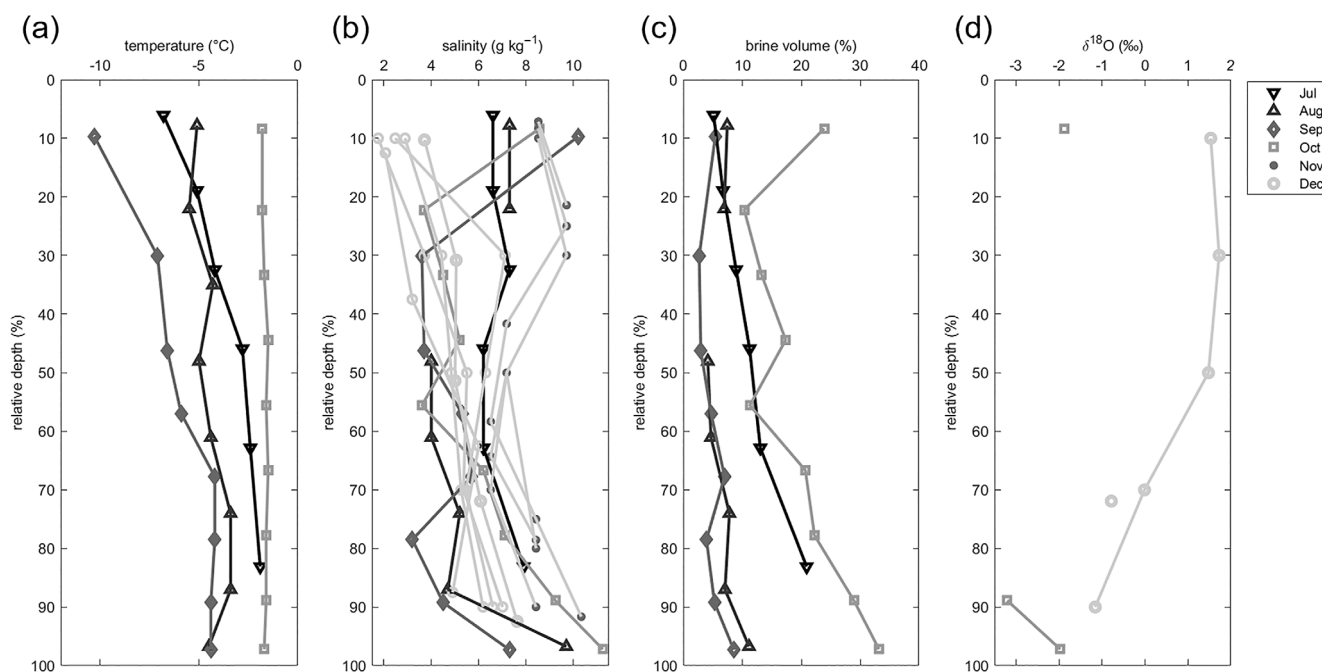
Fig. 2. Profiles of (**a**) temperature (°C); (**b**) salinity (absolute; g kg^{-1}); (**c**) brine volume (%); (**d**) $\delta^{18}O$ (‰) as a function of relative ice core depth (%) with symbols depicting sampling month. The sea-ice thickness, or ice core length (Table 2), is used as an absolute value (100%) to determine the relative depth of the physical measurements for the vertical ice core profiles. Due to the variability in sea-ice thickness, relative depths are used to enable clearer comparisons of seasonality at specific depth intervals, for example, sea-ice interface (relative depth 90–100%). Relative depths of the measurements in each ice core are marked by the different seasonal symbols (see legend). Plots were created using Matlab version R2017b.

(10.98 mmol m^{-2}) in September. Depth-integrated PO$_4$ peaked at 0.50 mmol m^{-2} at the end of December. From early November, bulk ice Si(OH)$_4$ and PO$_4$ increased slightly in the interior around the slush layer at $\sim$ 30% depth.

Sea-ice POC and PN

Concentrations of sea-ice POC varied between 19 and 6191 μmol L^{-1} and generally increased from spring to summer with highest concentrations at the sea-ice interface in early December (Fig. 3e,f). Distributions of PN followed a similar pattern, with concentrations between 1 and 443 μmol L^{-1} that increased from spring to summer at the base of the ice. Similar to the distributions of Si(OH)$_4$ and PO$_4$, concentrations of POC increased to 633 μmol L^{-1}, and PN increased to a maximum of 56 μmol L^{-1} in the interior ice around the slush layer in early November. In the upper part of the ice, POC and PN remained below 250 and 12 μmol L^{-1}, respectively, in spring and summer. Depth-integrated POC and PN were highest at 574 and 41 mmol m^{-2}, respectively, in early December (Table 2).

Sea-ice carbonate chemistry

The distributions of alkalinity and DIC (Fig. 3g,h) largely followed that of salinity, with high concentrations (> 500 μmol kg^{-1}) in the upper 30% of the ice during winter and early spring. Highest alkalinity and DIC of 1049 and

871 μmol kg^{-1}, respectively, occurred in the upper part of the ice in August. From late November, alkalinity and DIC decreased rapidly in the lower layers, followed by further decreases to minima of < 100 μmol kg^{-1} throughout the ice in summer. The Alk : DIC ratio was relatively homogenous at 1.0–1.2 from winter to spring throughout the ice (Fig. 3i), increasing to 1.2–1.6 by late November and peaking in summer (> 1.8) in the lower ice (Fig. 3g). Depth-integrated alkalinity and DIC were highest at 414 and 388 mmol m^{-2} in September and steadily decreased to lowest values of 93 and 60 mmol m^{-2}, respectively, by mid-December (Table 2). Between October and mid-November, alkalinity and DIC increased around the slush layer and in the upper 10–50% of the ice.

Ice-algal pigments

Chlorophyll *a* (Chl *a*) was used as a proxy for autotrophic biomass of ice algae. Chl *a* concentrations were low (< 1 μg L^{-1}) in winter sea ice with increases during spring and maximum concentrations (746 μg L^{-1}) at the base of the landfast ice in early summer (Fig. 3j). The winter community was a mixed assemblage of flagellates and diatoms. A seawater infiltration and slush layer developed from surface melt and flooding, where elevated Chl *a* concentrations (195 μg L^{-1}) were found in the ice interior from November. Depth-integrated Chl *a* ranged from < 0.5 mg m^{-2} in winter
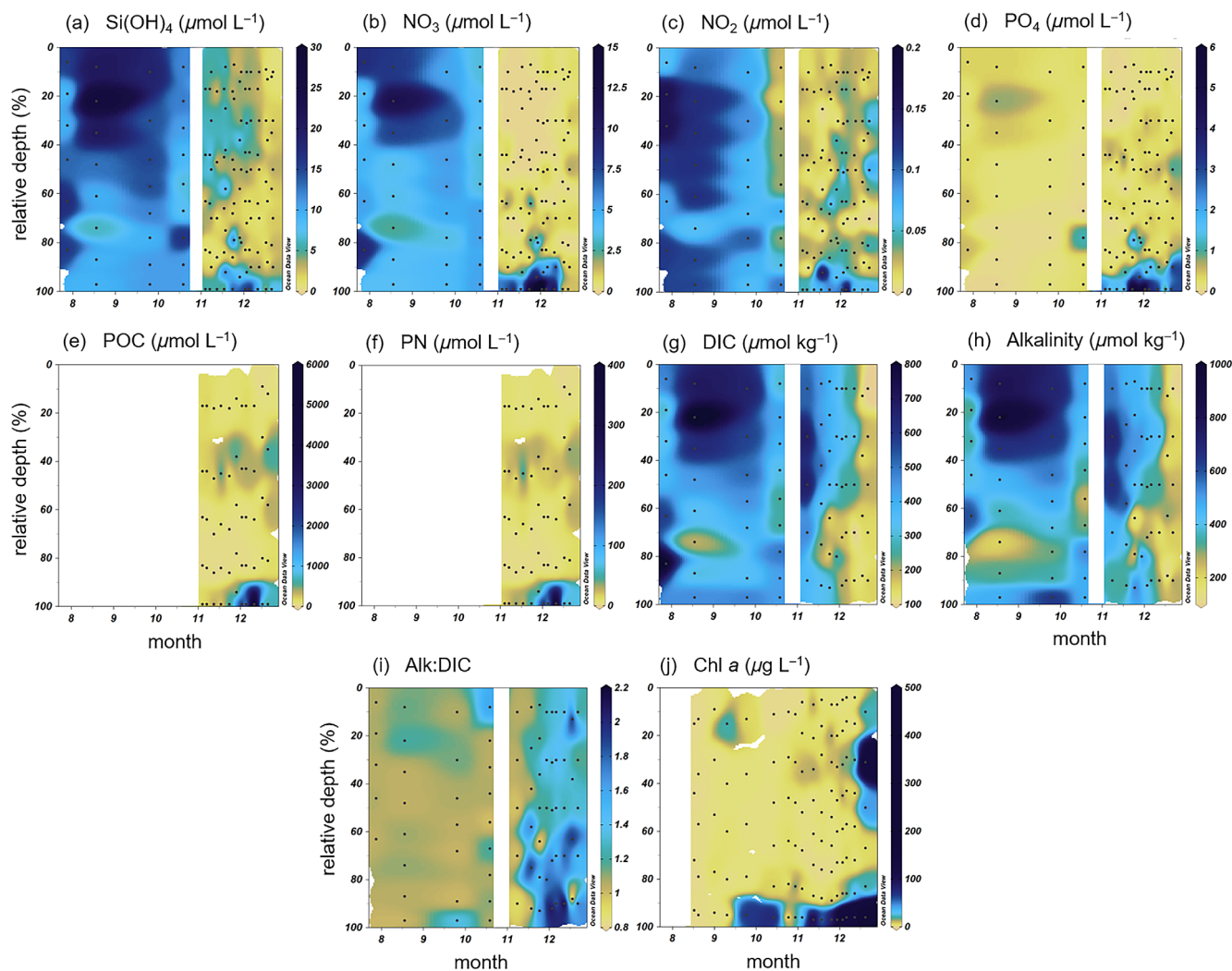
Fig. 3. Distributions of sea-ice (**a**) $Si(OH)_4$ ($\mu mol\ L^{-1}$); (**b**) NO_3 ($\mu mol\ L^{-1}$); (**c**) NO_2 ($\mu mol\ L^{-1}$); (**d**) PO_4 ($\mu mol\ L^{-1}$); (**e**) POC ($\mu mol\ L^{-1}$); (**f**) PN ($\mu mol\ L^{-1}$); (**g**) alkalinity ($\mu mol\ kg^{-1}$); (**h**) DIC ($\mu mol\ kg^{-1}$); (**i**) alkalinity and DIC ratio (Alk : DIC); (**j**) Chl *a* ($\mu g\ L^{-1}$) as a function of relative ice core depth (%). The sea-ice thickness, or ice core length (Table 2) is used as an absolute value (100%) to determine the relative depth of the biogeochemical and biological measurements for the vertical ice core profiles. Due to the variability in sea-ice thickness, relative depths are used to enable clearer comparisons of seasonality at specific depth intervals, for example, sea-ice interface (relative depth 90–100%). Relative depths of the measurements in each ice core are marked by black dots. Vertical white bars indicate a break in the time series (no data); for (**a**–**d**) and (**g**–**i**) this marks the transition between the July–October 2015 and November–December 2014 cores. Plots were created with Ocean Data View 4 (http://odv.awi.de) and spatial and temporal interpolation used for data visualization (Schlitzer 2018).

to 66.5 mg m^{-2} in summer (Table 2). Most of the ice algal biomass was detected in the lower 10% of the ice (the sea-ice interface). Accessory pigments fucoxanthin (Fuco), 19′-hexanoyloxyfucoxanthin (Hexa) and alloxanthin (Allo) exhibited distinct seasonality in depth-integrated concentrations (Table 2). The main photosynthetic pigment Fuco ranged from < 0.10 to 36.69 mg m^{-2} from winter to summer. This is indicative of a diatom-dominated community in December. The linear relationship between Fuco and Chl *a* was strong with Fuco/Chl *a* of 1.79 ± 0.02 mg m^{-2} ($r^2 = 1.00$; $p << 0.001$). The pigment Hexa is associated with haptophytes such as the prymnesiophyte *Phaeocystis*

antarctica and gradually increased from < 0.01 mg m^{-2} in August to a maximum of 0.63 mg m^{-2} in December. Ice around the slush layer in November had elevated concentrations of Hexa. The pigments Fuco and Hexa were not significantly correlated ($p > 0.05$), suggesting that they represent independent taxa. The elevated concentrations of Allo in September indicated the presence of cryptophytes.

Coupling of carbon, nutrients, and organic matter in sea ice

The relationships between DIC, nutrients and Chl *a* displayed variable patterns and some coupling between
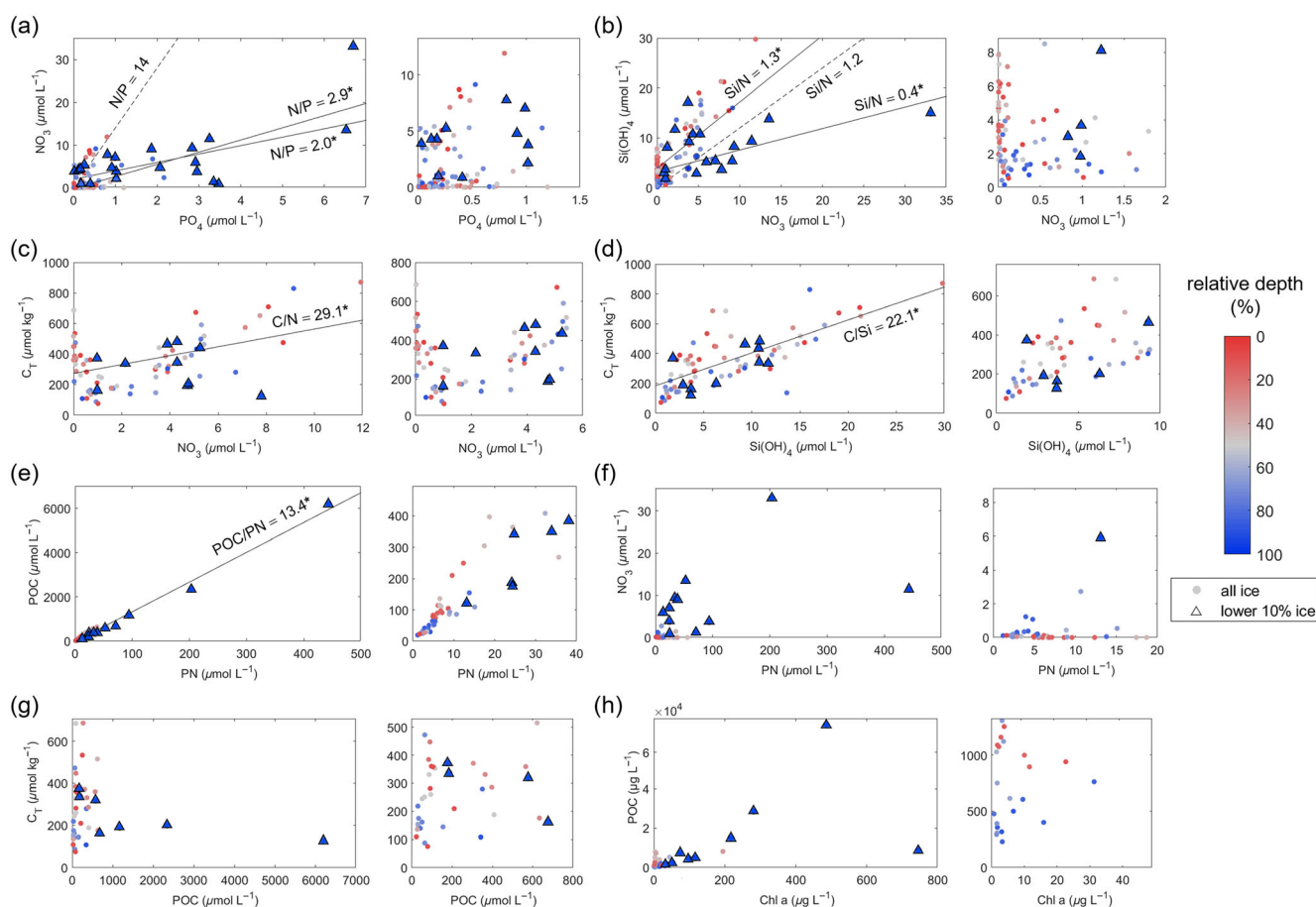
Fig. 4. Relationship of (**a**) NO_3 (μmol L^{-1}) and PO_4 (μmol L^{-1}); (**b**) $Si(OH)_4$ (μmol L^{-1}) and NO_3 (μmol L^{-1}); (**c**) DIC (μmol kg^{-1}) and NO_3 (μmol L^{-1}); (**d**) DIC (μmol kg^{-1}) and $Si(OH)_4$ (μmol L^{-1}); (**e**) POC (μmol L^{-1}) and PN (μmol L^{-1}); (**f**) NO_3 (μmol L^{-1}) and PN (μmol L^{-1}); (**g**) DIC (μmol kg^{-1}) and POC (μmol L^{-1}); (**h**) POC (μmol L^{-1}), and Chl a (μg L^{-1}) in sea ice. Key significant linear regression trends are indicated (*) for (**a**) winter–spring ice N/P = 2.0 and spring–summer ice N/P = 2.9, and the corresponding trend for seawater N/P = 14 for comparison; (**b**) winter–spring ice Si/N = 1.3 and spring–summer ice Si/N = 0.4, and the corresponding trend for seawater Si/N = 1.2 for comparison; (**c**) all seasons ice C/N = 29.1; (**d**) all seasons ice C/Si = 22.1; (**e**) all seasons ice POC/PN = 13.4. Smaller plots are expanded areas for each of the larger plots (linear regression trends not shown). Color indicates relative ice core depth (%) with triangles depicting the lower 10% of the ice. Plots were created using Matlab version R2017b.

the seasonal transitions and in the different depth ranges of the ice. The N/P ratio (Fig. 4a) varied from 1.97 ± 0.33 ($r^2 = 0.31$; $p < 0.001$) during the winter–spring transition to 2.86 ± 0.20 ($r^2 = 0.67$; $p << 0.001$) in spring–summer and showed deviation from seawater N/P ratios (~ 14) typical of this region (Pedulli et al. 2014; Henley et al. 2017). The Si/N ratio (Fig. 4b) varied from 1.33 ± 0.14 ($r^2 = 0.54$; $p << 0.001$) in winter–spring to 0.43 ± 0.07 ($r^2 = 0.29$; $p < 0.001$) in spring–summer and showed deviation from seawater ratios (~ 1.2; Henley et al. 2017). The DIC and NO_3 relationship (Fig. 4c) yielded an overall C/N of 29.14 ± 6.74 ($r^2 = 0.21$; $p < 0.001$), with large variability at low NO_3 concentrations that de-coupled the trends in spring and summer. For DIC and $Si(OH)_4$, the relationship (Fig. 4d) yielded C/Si of 22.08 ± 2.34 ($r^2 = 0.55$; $p << 0.001$) overall. The relationship between POC and PN showed that the organic nutrients were strongly coupled (Fig. 4e) with an overall POC/PN of

13.44 ± 0.21 ($r^2 = 0.99$; $p << 0.001$). The NO_3/PN relationship (Fig. 4f) was 0.05 ± 0.01 and variable but significant ($r^2 = 0.36$; $p < 0.001$). The relationship between inorganic and POC (Fig. 4g) was not statistically significant ($p = 0.28$), although low DIC corresponded to high POC in the lower 10% of the ice. The POC/Chl a ratios (Fig. 4h) were 4.39 ± 0.62 overall ($r^2 = 0.39$; $p << 0.001$), ranging from 10.9 at the ice base to extremely high ratios 1488–2070 in the interior ice from accumulation of ice algal POC relative to modest Chl a. The DIC/Chl a relationship (not shown) was not significant but elevated Chl a > 200 μg L^{-1} coincided with reduced DIC < 200 μmol kg^{-1} in the lower 10% of the ice.

Seasonality in inorganic carbon cycling in sea ice

Winter to summer inorganic carbon cycling within landfast sea ice was investigated using temporal changes in sea-ice DIC inventories between the different seasons (Table 4). A full sea-

Table 3. Seasonally averaged values and standard deviations of inorganic carbon and nutrients in the landfast sea ice in Hangar Cove (67.564°S, 68.130°W); summer averaged values and standard deviations in under-ice water in Hangar Cove; seasonally averaged values and standard deviations in surface water (0–5 m) in Ryder Bay (67.570°S, 68.225°W). Minimum and maximum values are in parentheses; n is number of measurements; — indicates no data.

Season Realm	Salinity	Si(OH)$_4$ μmol L^{-1}	NO$_3$ μmol L^{-1}	PO$_4$ μmol L^{-1}	Alkalinity μmol kg^{-1}	DIC μmol kg^{-1}	Alk : DIC
Winter	6.4 ± 1.6	14.2 ± 6.5	5.8 ± 2.8	0.3 ± 0.2	499 ± 236	487 ± 212	1.07 ± 0.05
Sea ice*	(4.0, 9.7)	(6.1, 29.8)	(2.4, 11.9)	(0.0, 0.8)	(204, 1049)	(186, 871)	(1.01, 1.21)
	$n = 14$	$n = 11$	$n = 10$	$n = 19$	$n = 13$	$n = 14$	$n = 13$
Spring	7.2 ± 2.2	6.4 ± 4.5	2.3 ± 2.9	0.5 ± 1.0	436 ± 133	401 ± 129	1.20 ± 0.26
Sea ice	(3.2, 11.2)	(0.1, 19.0)	(0.0, 13.5)	(0.0, 6.5)	(134, 711)	(139, 687)	(0.91, 1.91)
	$n = 37$	$n = 67$	$n = 65$	$n = 65$	$n = 39$	$n = 38$	$n = 38$
Summer	4.9 ± 1.6	3.4 ± 3.3	1.8 ± 5.0	0.7 ± 1.2	292 ± 111	200 ± 83	1.50 ± 0.38
Sea ice	(1.8, 7.6)	(0.5, 17.1)	(0.0, 33.1)	(0.0, 6.7)	(68, 479)	(75, 371)	(0.63, 2.28)
	$n = 24$	$n = 49$	$n = 49$	$n = 49$	$n = 24$	$n = 24$	$n = 24$
Summer	31.9 ± 2.5	54.2 ± 13.3	15.8 ± 9.3	1.7 ± 0.1	2094 ± 250	1896 ± 346	1.12 ± 0.11
Under-ice water	(28.7, 36.8)	(33.1, 66.6)	(1.5, 23.7)	(0.1, 1.7)	(1550, 2277)	(1144, 2144)	(1.06, 1.36)
	$n = 7$	$n = 7$	$n = 7$	$n = 7$	$n = 7$	$n = 7$	$n = 7$
Autumn	33.1 ± 0.1	54.5 ± 3.2	17.2 ± 1.9	1.4 ± 0.1	2253 ± 7	2120 ± 13	1.06 ± 0.01
Surface water * (ice forming)	(33.0, 33.2)	(50.2, 58.5)	(15.1, 20.5)	(1.2, 1.6)	(2249, 2268)	(2107, 2140)	(1.05, 1.07)
	$n = 7$	$n = 7$	$n = 7$	$n = 7$	$n = 7$	$n = 7$	$n = 7$
Winter	33.6 ± 0.3	55.6 ± 4.6	18.9 ± 5.2	1.6 ± 0.3	2285 ± 15	2152 ± 40	1.06 ± 0.02
Surface water * (ice cover)	(33.2, 33.8)	(50.2, 61.8)	(12.8, 26.2)	(1.4, 2.0)	(2265, 2303)	(2116, 2212)	(1.04, 1.08)
	$n = 5$	$n = 5$	$n = 5$	$n = 5$	$n = 5$	$n = 5$	$n = 5$
Spring	33.8 ± 0.1	72.7 ± 7.8	26.2 ± 4.0	1.7 ± 0.2	2297 ± 9	2168 ± 64	1.06 ± 0.04
Surface water (ice melt)	(33.6, 33.9)	(66.5, 81.5)	(23.8, 30.8)	(1.5, 1.8)	(2288, 2306)	(2098, 2224)	(1.03, 1.10)
	$n = 3$	$n = 3$	$n = 3$	$n = 3$	$n = 3$	$n = 3$	$n = 3$
Summer	33.2 ± 0.3	59.8 ± 13.3	17.5 ± 10.6	1.2 ± 0.6	2267 ± 14	2067 ± 100	1.09 ± 0.04
Surface water (ice free)	(32.6, 33.6)	(38.4, 71.5)	(0.3, 25.9)	(0.1, 1.8)	(2239, 2285)	(1916, 2172)	(1.05, 1.16)
	$n = 11$	$n = 11$	$n = 11$	$n = 11$	$n = 10$	$n = 11$	$n = 10$

*Cores and data from 2015.

ice life cycle is assumed, from formation in autumn/winter to complete ice melt in summer. The total change (ΔDIC_{ice}) was calculated from the differences in seasonal average sea-ice DIC-integrated values and represented the composite change in DIC resulting from changes in salinity (ΔDIC_{sal}) due to brine rejection, concentration and meltwater dilution; organic matter production/remineralization (ΔDIC_{bio}); ikaite precipitation/dissolution (ΔDIC_{CaCO3}); residual changes (ΔDIC_{res}) determined from the difference between ΔDIC_{ice} and all other ΔDIC contributions.

To remove effects of salinity changes, DIC was normalized ($\Delta DIC_{6.4}$) to the mean bulk sea-ice salinity in winter (6.4; Table 3) following the standard technique in Friis et al. (2003). Changes due to salinity effects were then estimated from $\Delta DIC_{sal} = \Delta DIC_{ice} - \Delta DIC_{6.4}$. Taking NO$_3$ as a proxy for biological production (Fransson et al. 2011), the seasonal changes in sea-ice NO$_3$ concentrations were converted to DIC (ΔDIC_{bio}) using both the C : N uptake ratio of 6.625 ($\Delta DIC_{bio6.6}$) from Redfield et al. (1963) and the POC : PN of

13.4 ($\Delta DIC_{bio13.4}$) estimated from organic carbon and nutrient cycling during this study (Fig. 4e). Caveats using NO$_3$ as a proxy include introducing uncertainty as a result of other NO$_3$ transformations, for example, denitrification, and exchanges in the semi-closed ice system, as discussed previously (Henley et al. 2012). Changes in DIC due to ikaite precipitation/dissolution (ΔDIC_{CaCO3}) were estimated from changes in potential alkalinity (salinity-normalized alkalinity plus salinity-normalized nitrate) following Jones et al. (2017). The ΔDIC_{res} value accounts for the residual change in DIC, for example, other processes such as inputs of DIC and organic matter (subsequently remineralized to release DIC) by seawater infiltration and air-ice CO$_2$ exchange.

The seasonal changes in sea-ice DIC showed that the landfast sea ice was a sink of DIC up to 0.173 mol m^{-2} during the sea-ice cycle from the period of ice formation to ice melt (Table 4). Changes in the sea-ice DIC inventories during the winter–spring transition were dominated by uptake during primary production by the sympagic community. The spring–

Table 4. Seasonal changes in DIC (mol m^{-2}) in landfast sea ice in Hangar Cove (67.564°S, 68.130°W). The total change (ΔDIC_{ice}) is the difference in the DIC inventory from average integrated values in winter, spring, and summer seasons and represents the composite seasonal change (winter–summer). The ΔDIC_{ice} is driven by salinity changes (ΔDIC_{sal}), organic matter production/remineralization using Redfield et al. ([1963](#)) C : N ratio ($\Delta DIC_{bio6.6}$) and POC : PN ratios from this study ($\Delta DIC_{bio13.4}$), ikaite precipitation/dissolution (ΔDIC_{CaCO3}) and residual changes (ΔDIC_{res}) from other processes (residuals determined using $\Delta DIC_{bio6.6}$ and $\Delta DIC_{bio13.4}$).

	ΔDIC_{ice} mol m^{-2}	ΔDIC_{sal} mol m^{-2}	$\Delta DIC_{bio6.6}$ mol m^{-2}	$\Delta DIC_{bio13.4}$ mol m^{-2}	ΔDIC_{CaCO3} mol m^{-2}	ΔDIC_{res} mol m^{-2}
Winter–spring	−0.004	0.022	−0.013	−0.027	−0.005	−0.008 / 0.006
Spring–summer	−0.169	−0.028	−0.008	−0.015	−0.061	−0.073 / -0.065
Winter-summer	−0.173	−0.005	−0.021	−0.042	−0.066	−0.081 / -0.060

summer changes showed that ikaite precipitation and other losses, for example, CO_2 release from the ice, were key processes influencing sea-ice DIC. Salinity-driven changes in DIC showed increases (0.022 mol m^{-2}) followed by decreases (−0.028 mol m^{-2}) in winter–spring and spring–summer, respectively. The seasonal transitions indicated general DIC loss due to other processes such as CO_2 outgassing from the ice (ΔDIC_{res}). Estimated increases in DIC from winter to spring coincided with increased sea-ice DIC associated with salinity changes. Residuals in ΔDIC_{ice} were smaller when $\Delta DIC_{bio13.4}$ was used, which indicated that the POC : PN uptake ratio was more suitable than the C : N Redfield ratio for carbon and nutrient cycling in sea ice.

Under-ice water biogeochemistry

Average salinity of under-ice water during summer was 31.9 ± 2.5 g kg^{-1} (Table 3), ranging from 36.8 on 12 December (likely due to a residual brine-mixed meltwater) to 28.7 on 18 December (Fig. 5a). Prior to notable ice melt in early December, salinity was lower compared with surface waters in Ryder Bay and decreased from about 33.6 to 32.6 from December to January. Values of $\delta^{18}O$ (Fig. 5b) tended to become lower during December, ranging from 1.55‰ to −1.16‰, as evidence of increasing contributions of meteoric water (glacial meltwater, snow). During the same period, changes in $\delta^{18}O$ in Ryder Bay were more subtle, ranging from −1.02‰ to −0.54‰. Isotopic values were lighter (−3.34‰) in the saline meltwater, which indicated a mixture of meteoric water and residual brine.

At the beginning of December, DIC and alkalinity in the under-ice water were 2125–2144 and 2249–2277 μmol kg^{-1}, respectively, and similar to those concentrations in Ryder Bay (Fig. 5c,d). Values of alkalinity and DIC were reduced rapidly to 1550 and 1144 μmol kg^{-1}, respectively, in the lower-salinity meltwater in mid-December. Salinity-normalized alkalinity and DIC$_{sal}$ were also lowest at 1801 and 1329 μmol kg^{-1}, respectively, at this time, after which salinity-normalized alkalinity was higher than oceanic concentrations (Fig. 5d). The Alk : DIC ratio varied from average values of ~ 1.06 in early December to 1.05 (1.36) in the higher (lower) salinity waters

(Fig. 5e). Concentrations of Si(OH)$_4$, NO$_3$, and PO$_4$ were highest at 66.6, 23.7, and 1.65 μmol L^{-1}, respectively, in early December (Fig. 5f–h). Compared with surface waters of Ryder Bay, Si(OH)$_4$ and NO$_3$ had similar concentrations whereas PO$_4$ was slightly higher in the under-ice water. Rapid reductions in under-ice water Si(OH)$_4$, NO$_3$, and PO$_4$ to 33.1[1], 11.3, and 1.03 μmol L^{-1}, respectively, were concurrent with lowest DIC and alkalinity by mid-December. Continued drawdown of NO$_3$ and PO$_4$ to lowest levels of 1.5 and 0.12 μmol L^{-1}, respectively, occurred in January.

Discussion

Winter sea ice: A conceptual model for seasonal biogeochemical cycling

Landfast sea ice in Hangar Cove formed in May–June, which was characteristic for this region of the West Antarctic Peninsula (Meredith et al. [2008](#)). Following the colder period in July and August, brine volume increased (5–9%) above threshold levels for percolation and transport in the ice and increased porosity allowed movement and exchange of liquids and dissolved constituents (Golden et al. [1998](#)). The thermohaline characteristics showed colder and more saline upper ice, warmer and fresher interior ice, and warmer and more saline lower ice, which were similar to those previously reported in Antarctic landfast sea ice (van der Linden et al. [2020](#)) and pack ice during the winter (Fripiat et al. [2017](#)).

Nutrient and carbon-rich Circumpolar Deep Water (CDW) transported across the shelf of the West Antarctic Peninsula preconditions coastal waters with inorganic nutrients for the productive season that follows (Henley et al. [2017](#)). Combined with localized nutrient cycling, these processes characterize the biogeochemistry of source waters for locally formed landfast sea ice (Henley et al. [2012](#), [2017](#); Jones et al. [2017](#)). During formation, alkalinity, DIC and macronutrients were largely expelled from the sea ice, characterizing the ice with lower concentrations compared with winter surface waters, and a fraction likely became concentrated in brines in channels and pockets within the ice matrix (Rysgaard et al. [2007](#); Dieckmann et al. [2008](#)). Brine is typically rejected from the
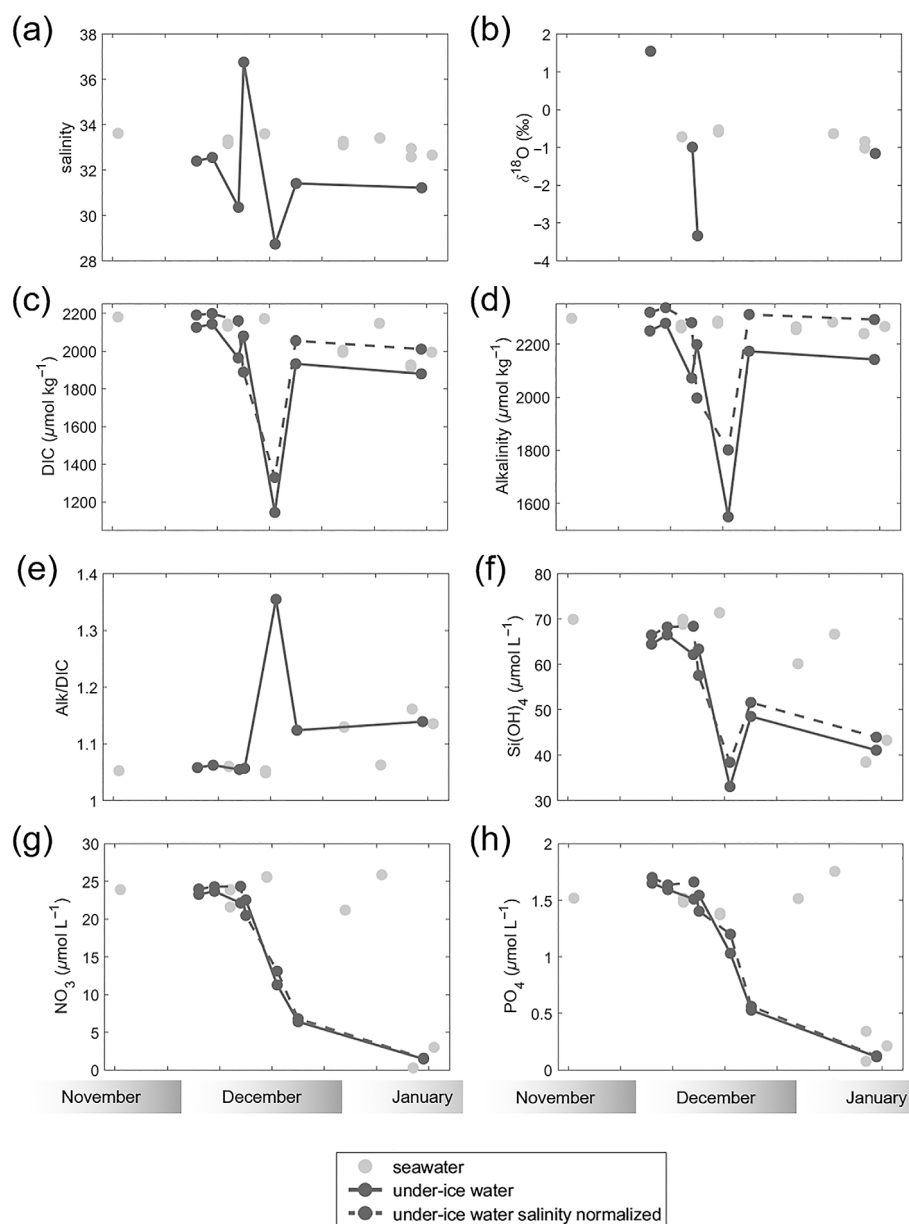
Fig. 5. Temporal changes in (**a**) salinity; (**b**) $\delta^{18}O$ (‰); (**c**) DIC (μmol kg^{-1}); (**d**) alkalinity (μmol kg^{-1}); (**e**) Alk : DIC ratio; (**f**) Si(OH)$_4$ (μmol L^{-1}); (**g**) NO$_3$ (μmol L^{-1}); (**h**) PO$_4$ (μmol L^{-1}) in surface seawater (0–5 m) of Ryder Bay (gray dots), under-ice water (black dots and solid line), and salinity-normalized under-ice water values (black dots and dashed line) during late spring (November) and summer (December–January). Shading (white to gray) in the month labels corresponds to temporal progression throughout each month. Plots were created using Matlab version R2017b.

growing sea ice into the underlying seawater (Rysgaard et al. 2007; Dieckmann et al. 2008); however, some can be encapsulated within the ice (Fripiat et al. 2017; Vancoppenolle et al. 2013) and would therefore contribute to variability in chemical properties of spring and summer ice during the melt period.

The landfast sea ice in winter exhibited higher alkalinity and DIC relative to the other seasons (Fig. 6a) and accompanied by elevated salinity-normalized alkalinity and DIC, which are independent of physical effects, showed

pronounced seasonality in biogeochemical processes within the ice (Fig. 6b–e). Higher salinity-normalized alkalinity and DIC also coincided with high values of NO$_{3sal}$ and Si(OH)$_{4sal}$ in August, which were similar to and in several cases higher than concentrations in winter surface waters in Ryder Bay (Henley et al. 2017; Legge et al. 2017). Removing effects of salinity changes, enrichment of the inorganic carbon and nutrient pool in winter sea ice compared with seawater likely resulted from a combination of concentration, transport, and redistribution of brines (Vancoppenolle et al. 2013), followed
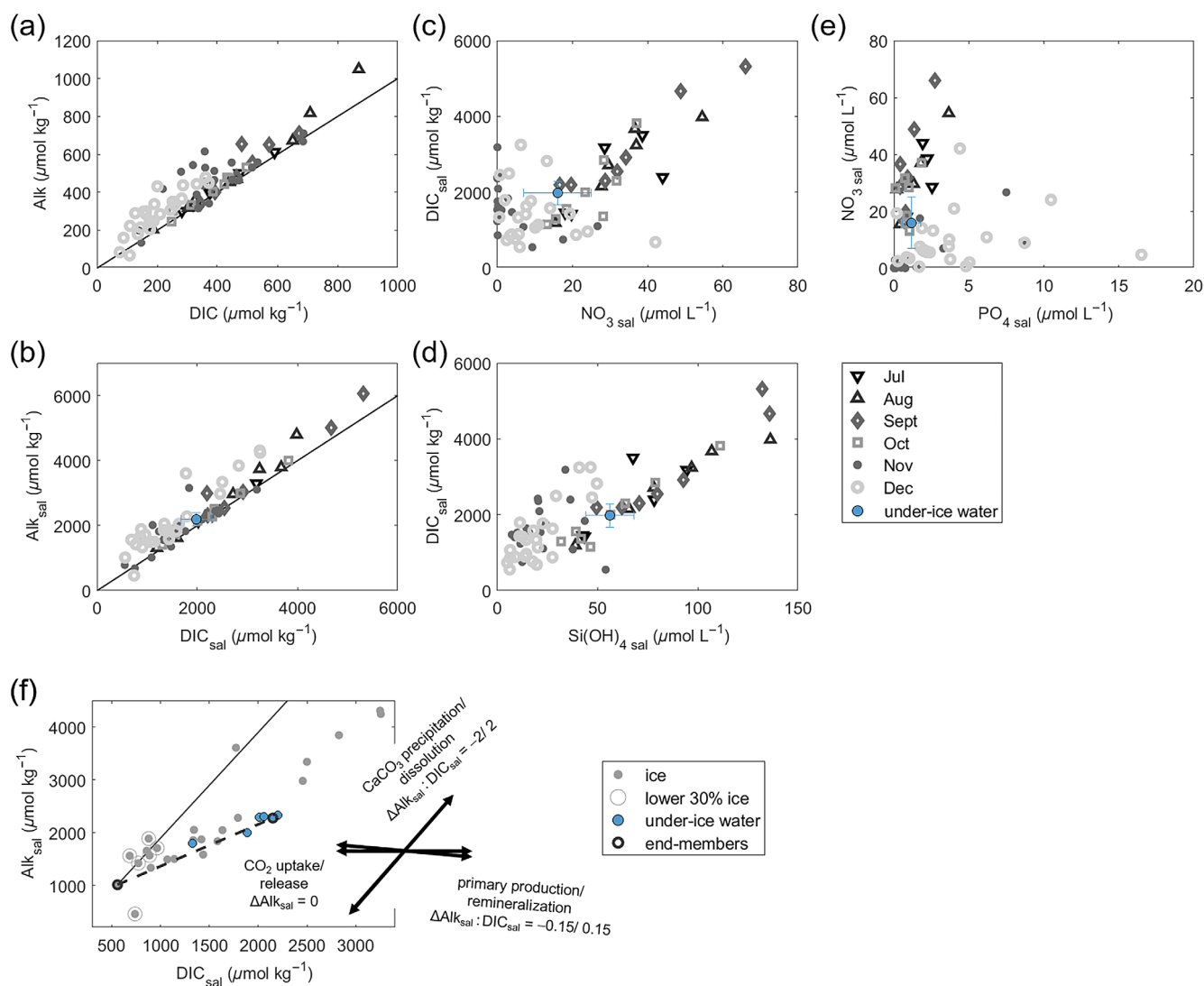
Fig. 6. Relationship of seasonal sea-ice (**a**) alkalinity (Alk; μmol kg^{-1}) and DIC (μmol kg^{-1}); (**b**) salinity-normalized alkalinity (Alk$_{sal}$; μmol kg^{-1}) and DIC$_{sal}$ (μmol kg^{-1}); (**c**) DIC$_{sal}$ (μmol kg^{-1}) and NO$_{3sal}$ (μmol L^{-1}); (**d**) DIC$_{sal}$ (μmol kg^{-1}) and Si(OH)$_{4sal}$ (μmol L^{-1}); (**e**) NO$_{3sal}$ (μmol L^{-1}) and PO$_{4sal}$ (μmol L^{-1}) with symbols depicting sampling month. A 1 : 1 trend line (black) is included for reference in (**a**) and (**b**) and salinity-normalized values for summer under-ice water averages ($n = 7$; closed blue circles) and standard deviations (error bars) are shown in (**b**) to (**e**). Relationships of summer Alk$_{sal}$ (μmol kg^{-1}) and DIC$_{sal}$ (μmol kg^{-1}) in sea ice (closed gray circles), lower 30% of the ice (open circles) and under-ice water (closed blue circles) are shown in (**f**). Trend lines in (**f**) show theoretical mixing (black dashed line) between endmember values (black open circles) of summer sea ice and ice-free surface waters in Ryder Bay and the 2 : 1 relationship (black solid line) of ikaite precipitation/dissolution. Insert arrows in (**f**) depict the influence of key processes on Alk$_{sal}$ and DIC$_{sal}$ adapted from Papadimitriou et al. (2012). Plots were created using Matlab version R2017b.

by intense remineralization of seawater-derived organic matter due to heterotrophic activity in the closed or semi-closed ice system (Fripiat et al. 2015). Seasonal maxima in NO$_2$ (an intermediate in biological nitrogen cycling) further supported the winter sea-ice nutrient patterns as nitrification by the active over-wintering microbial community would enrich NO$_2$, following ammonium production (not assessed in this study) from the organic matter decay (Henley et al. 2017). A notable feature was the low PO$_4$ concentrations ($\sim 0.3\ \mu$mol L^{-1}) in winter sea ice relative to the concentrations of NO$_2$, NO$_3$, and Si(OH)$_4$ (Fig. 6e). Sea-ice PO$_4$ in winter

was depleted in comparison with surface water PO$_4$ concentrations in autumn ($\sim 1.4\ \mu$mol L^{-1}) and winter ($\sim 1.6\ \mu$mol L^{-1}) (Table 3). The biogeochemical cycling of the three main macronutrients (NO$_3$, PO$_4$, Si(OH)$_4$) became de-coupled as the seasons progressed; bulk sea-ice PO$_4$ increased and NO$_3$ and Si(OH)$_4$ decreased. Despite freshening and biological uptake, summer sea-ice PO$_4$ was approximately twice as high (average $\sim 0.7\ \mu$mol L^{-1}) relative to winter sea ice.

Cold temperatures (-10.3°C) at the air-ice interface in September lowered the ice porosity and presented ideal conditions to promote ikaite precipitation (Jones and Coote 1981;
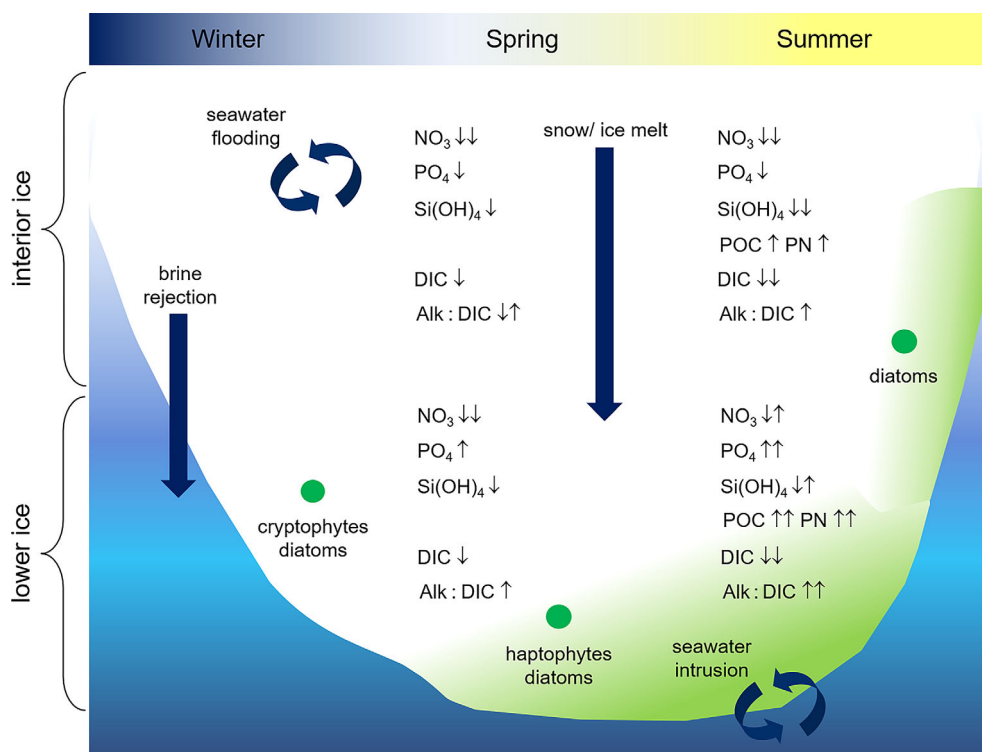
Fig. 7. Schematic of the conceptual model for carbon and nutrient cycling in landfast sea ice during the winter–spring and spring–summer transitions. Relative seasonal changes in the interior (20–80% relative ice core depth) and lower (80–100% relative ice core depth) layers of the ice are shown for NO_3, PO_4, $Si(OH)_4$, DIC, Alk : DIC, POC, and PN. The distribution of biomass (Chl a) is approximated (green shading) and ice-algal community composition is shown (closed green circles). The direction and magnitude of relative seasonal changes are indicated (thin black arrows: increases ↑, strong increases ↑↑, decreases ↓, strong decreases ↓↓, variable changes ↓↑). Key physical processes are illustrated (thick dark blue arrows).

Dieckmann et al. 2008; Fransson et al. 2011; Brown et al. 2015; Moreau et al. 2015). The vertical distribution of DIC and alkalinity and seasonally low sea-ice Alk : DIC ratios strongly suggested that ikaite precipitation had taken place in the landfast ice during winter (Rysgaard et al. 2007; Fransson et al. 2011). The increased sea-ice Alk : DIC that followed the seasonal transitions from average values ∼ 1.07 in winter to average values ∼ 1.50 in summer, and elevated Alk : DIC in the ice relative to under-ice water and seawater of Ryder Bay, further indicated that formation of ikaite was important in driving winter inorganic carbon dynamics. Under-ice water was not sampled during winter and thus brine rejection and associated DIC and CO_2 transport could not be fully determined, but winter sea ice Alk : DIC ratios (Fig. 3i; Table 3) were used to infer ikaite processes within the ice (Fransson et al. 2011, 2013; Brown et al. 2015) during this period.

The co-occurrence of lower PO_4 concentrations and evidence of ikaite formation in winter landfast ice supported the potential role of ikaite in PO_4 variability, whereby co-precipitation of ikaite and PO_4 would scavenge PO_4 out of the winter ice (Hu et al. 2014). The patterns in sea-ice PO_4 in this study were similar both seasonally and vertically within the ice column to previous studies for Antarctic landfast sea ice

(van der Linden et al. 2020) and pack ice (Fripiat et al. 2017) that indicated that PO_4 depletion and ikaite precipitation may be linked. In addition, other processes may have contributed to differential partitioning of PO_4 in sea ice, such as the convective loss of NO_3, preferential remineralization of organic phosphorus, PO_4 adsorption onto biofilms (van der Linden et al. 2020) and formation of PO_4-rich biomolecules during sympagic blooms (Fripiat et al. 2017 and references therein).

The landfast sea ice present in Hangar Cove during winter–spring 2015 was thicker (0.77–0.93 m) compared with the ice in winter–spring 2014 (0.36–0.58 m). Year-to-year variability was not assessed during this study due to limited data from the winter–spring 2014 and 2015 sea ice, but the different ice thickness likely contributed to further variations in physical structure and properties of the ice. However, seasonal variations in physical, biogeochemical and biological characteristics are taken to exhibit the greatest temporal signals for a study period of about 12 months, as shown in Fripiat et al. (2017) presenting both seasonal and interannual variations in Antarctic sea ice inorganic nutrients and organic matter. Thus, the physicobiogeochemical processes occurring between the period of ice formation and the onset of ice melt can be used as a pseudo-seasonal time series to develop a conceptual model of inorganic

carbon and nutrient dynamics during the winter–spring and spring–summer transitions (Fig. 7).

Spring dynamic shifts in sympagic algae and carbon and nutrient uptake

The winter–spring transition was a period of rapid change in the physical and biogeochemical characteristics of the landfast sea ice. The emergence of cryptophytes in early September indicated that conditions were most likely heterotrophic, consistent with low light availability that is typical during the Antarctic spring (van Leeuwe et al. 2018). Increasing light levels exerts a strong control on the accumulation of ice-algal biomass (Thomas and Dieckmann 2010; van Leeuwe et al. 2018) and likely promoted the development of autotrophic ice-algal blooms (van Leeuwe et al. 2022) that reduced the winter stocks of inorganic carbon and nitrate in the ice. This was evident from the closer coupling and significant reduction of NO_3 and DIC in the ice interior relative to surface waters.

Warmer conditions by October reshaped the physicochemical conditions as the ice became relatively isothermal with temperatures in the upper ice up to $-1.5°C$ and increased brine volumes ($> 20\%$) indicated increased porosity (Golden et al. 1998). Ikaite formation and transport of brines redistributed salt and inorganic carbon in the sea ice, leading to high and variable alkalinity and DIC in the upper and interior ice. Isotopically light $\delta^{18}O$ was indicative of snow melt that percolated through the permeable ice matrix, which would enhance the meteoric signal ($-3.21‰$) towards the ice base. Any ikaite minerals could be flushed out of the upper layers and imprint a signal of reduced alkalinity and DIC in the interior and lower ice layers. Furthermore, any ikaite trapped in the ice would dissolve during analysis to yield a signal of excess alkalinity (Fransson et al. 2013), thus contributing to variable Alk : DIC ratios.

Vertical gradients showed high alkalinity and DIC ($> 500\ \mu mol\ kg^{-1}$) in the upper 30% of the ice that decreased to variable and lower values ($< 300\ \mu mol\ kg^{-1}$) in the interior and lower layers as a signal of previous ikaite formation, brine drainage and re-distribution of dissolved minerals (Vancoppenolle et al. 2013), dilution and biological carbon uptake as the ice started to melt (Fig. 6f). Increases in Alk : DIC ratios (1.2–1.6) and macronutrient concentrations in the lower ice in late November indicated a seasonal shift in inorganic carbon dynamics as dissolution of ikaite in the melting sea ice, combined with remineralization of organic matter, had taken place (Papadimitriou et al. 2012; Fripiat et al. 2017).

Melting sea ice and dissolution of biogenic silica from sympagic diatoms in the brine channels (Fripiat et al. 2017) likely contributed to increased $Si(OH)_4$ in the lower ice during spring. Biogenic silica dissolution occurs at a slower rate than organic matter remineralization, but both processes are happening concurrently (Fripiat et al. 2017). As the ice warmed and became more porous, intrusions of nutrient-rich seawater

at the sea-ice interface would increase macronutrient concentrations, which is in broad agreement with increased NO_3 and PO_4 concentrations in the lower ice. However, the uncoupling with DIC and alkalinity (reduced DIC and alkalinity values in lower ice during spring) indicated that other processes including organic matter remineralization and biogenic silica frustule dissolution were key in driving inorganic nutrient dynamics in the lower ice.

Snow accumulation on landfast ice can depress the ice below the sea surface and cause flooding, where subsequent infiltration and freeze–thaw cycles can form a highly variable interstitial layer (Jeffries et al. 1998). Visual and biogeochemical observations indicated that surface flooding had occurred in October/November and formed a slush layer. This provided a mechanism for pelagic phytoplankton and seawater-derived salt, inorganic carbon, macronutrients, and organic matter to infuse the interior ice resulting in variable $Si(OH)_4$, PO_4, and Chl *a* and fluctuations in POC, PN, alkalinity, and DIC (Fig. 3). Elevated concentrations of Hexa indicated that the sympagic community had shifted and haptophytes, for example, *Phaeocystis*, colonized the interstitial layer. Bulk sea-ice DIC showed variable decreases with increased ice-algal biomass, suggesting that any NO_3 replenished by seawater flooding fueled ice-algal productivity, biological DIC uptake and organic matter production (Günther and Dieckmann 1999; Papadimitriou et al. 2012; Arrigo et al. 2014). Variability in sea-ice alkalinity (and to a lesser extent DIC) around the slush layer resulted from dilution effects from sea-ice meltwater, enrichment from seawater flooding and the imprint of ikaite mineral dynamics.

The POC/Chl *a* ratio also increased in the upper and interior ice as concentrations of POC increased rapidly with modest increases in Chl *a* in the presence of the haptophyte community. Seawater flooding and close proximity to land can also influence nutrient and organic matter cycling in landfast sea-ice through additional inputs of detrital-derived and terrestrially derived organic matter that could contribute to the observed accumulated POC and elevated POC/Chl *a* ratios (Gleitz and Thomas 1993; Henley et al. 2012). At this time, NO_2 comprised $\geq 60\%$ of the total $NO_3 + NO_2$ pool and suggested that intense organic matter recycling had also taken place. Infiltration layers in Antarctic landfast ice are known to provide favorable habitats for microorganisms as the seawater replenishes inorganic nutrients and, in favorable light conditions, promotes sympagic production (van Leeuwe et al. 2018 and references therein), as shown for the landfast sea ice in Hangar Cove during spring.

Substantial sea-ice melt, ice-algal biomass, and biogeochemical cycling during summer

Continued melting, meltwater dilution, and biotic and abiotic processes characterized the summer sea ice with low NO_3, $Si(OH)_4$, and DIC, variable alkalinity and elevated PO_4 (Figs. 3, 6b–d). The isotopically lighter and more saline lower ice layers

indicated that percolating snowmelt and some exchange with the underlying water influenced the physicochemical environment. The lower ice, and particularly the sea-ice interface, was very productive using the proxy of the Chl *a* seasonal maximum of 746 μg L^{-1} as an indicator of substantial algal biomass, with an accompanying reduction of DIC to minimum values of 65 μmol kg^{-1} and accumulation of POC to 6191 μmol L^{-1}. Similarly, significant increases in algal biomass and POC were recently reported for summer Antarctic landfast ice (van der Linden et al. 2020). Highest concentrations of PN of 443 μmol L^{-1} were also found in the lower ice and at the sea-ice interface, with similar concentrations to those in productive Antarctic pack ice (Fripiat et al. 2017). The sea-ice POC concentrations were about 100 times higher than seawater concentrations in Ryder Bay (Henley et al. 2012), which showed that the landfast sea ice was an efficient biological sink of DIC and inorganic nutrients through assimilation into organic matter. Higher POC concentrations generally synchronized with higher Chl *a* concentrations and values were very similar to those reported previously (Gleitz and Thomas 1993; Fransson et al. 2011; Henley et al. 2012). The sea-ice Chl *a* was substantially higher than Chl *a* concentrations in the pelagic phytoplankton blooms in Ryder Bay, which exhibited seasonal maximum values up to ~ 35 μg L^{-1} (van Leeuwe et al. 2020). The POC/PN ratios of 13.44 were typical for sympagic microalgae and consistent with the preferential degradation of organic nitrogen over carbon, NO$_3$-poor algal metabolism and/or influence of exopolymeric substances (Gleitz and Thomas 1993; Meiners et al. 2004). These features are characteristic of (semi-)closed sea-ice systems (Fransson et al. 2011; Henley et al. 2012) where autotrophic fixation led to greater DIC (and CO$_2$) and nutrient drawdown compared with open systems of ice-free surface waters.

Rapid Si(OH)$_4$ drawdown alongside increased concentrations of Chl *a* and Fuco reflected the succession of the diatom community, whereby Si(OH)$_4$ depletion occurred about 1 month later than NO$_3$. As for patterns in summer Antarctic pack ice (Fripiat et al. 2017), the Si(OH)$_4$ concentrations in landfast sea ice were lower compared with surface waters in spring and summer. Transient sea-ice Si(OH)$_4$ limitation could be expected to occur in blooming summer sympagic communities that are dominated by diatoms. The shift toward lower N/P uptake ratios (< 1 in spring–summer) and synchronicity in the cycling of Si(OH)$_4$ and NO$_3$ were indicative of diatom production (Clarke et al. 2008) under nutrient-replete conditions in the ice (Brzezinski 1985). The closer coupling between Si(OH)$_4$ and DIC, compared with NO$_3$ and DIC, suggested more efficient inorganic carbon uptake occurred in the diatom community particularly in the lower layers of the landfast ice. The lower Si/N uptake ratios (average ~ 0.4) in the lower ice layers implied that faster rates of organic matter remineralization (releasing NO$_3$) than biogenic silica dissolution (releasing Si(OH)$_4$) had taken place. Concurrent higher Si/N uptake

ratios (average ~ 1.2) in surface waters of Ryder Bay, typical for this region during the growing season (Si/N of 1.2–1.4; Henley et al. 2017), further indicated that seawater flushing and infusion of seawater-derived Si(OH)$_4$ and NO$_3$ was likely minor during the summer compared with spring.

The seasonal shifts in sea-ice NO$_2$ distributions followed a similar pattern to NO$_3$, increasing from relatively low concentrations that comprised $\sim 2\%$ of the inorganic nitrogen pool in winter to $\sim 31\%$ of the total inorganic nitrogen in spring and summer. Vertical gradients showed that NO$_2$ represented a smaller fraction of 1–7% of the total inorganic nitrogen in the lower ice layers and suggested that primary production at the bottom of the ice was supported by intense organic matter recycling, with contributions from the underlying seawater being minor (Henley et al. 2012; Fripiat et al. 2017). The weak coupling between NO$_3$ and PO$_4$ and general lower N/P ratios in the lower ice resulted from intense NO$_3$ drawdown and PO$_4$ accumulation. Unlike near-total depletion of NO$_3$ and Si(OH)$_4$, summer sea-ice PO$_4$ concentrations exceeded concentrations in the under-ice water and surface waters of Ryder Bay (Fig. 5h; Table 3). The seasonality in sea-ice PO$_4$ further supported the notion of a different type of biogeochemical cycling controlling PO$_4$ distributions. Mechanisms of PO$_4$ enrichment in landfast sea ice during the seasonal transitions that led to an imbalance in production and consumption processes by the summer could include adsorption onto biofilms (Arrigo et al. 1995; Meiners et al. 2004; Cozzi 2008; van der Linden et al. 2020), preferential remineralization (Fripiat et al. 2017), and excess PO$_4$ released upon ikaite dissolution following the co-precipitation of PO$_4$ with ikaite during the preceding winter (Hu et al. 2014; Fripiat et al. 2017). In addition, potential release of inorganic compounds including PO$_4$ could occur from cell lysis (Fripiat et al. 2017; Torstensson et al. 2018), assumed to be insignificant due to the decoupling of PO$_4$ patterns with NO$_3$ and Si(OH)$_4$ in this study as discussed earlier.

A rise in the 5% brine volume threshold from the lower to upper part of the ice increases brine channel connectivity and sea-ice permeability (Vancoppenolle et al. 2013), which enabled meltwater flushing and reduced brine volume in the landfast sea ice. Inclusions of brine at or near the ice base are more connected with the underlying ocean to allow brine drainage, seawater infiltration, and brine-seawater exchange. Brine drainage is an efficient transport mechanism of DIC, and other dissolved constituents, from the sea ice to the underlying seawater (Rysgaard et al. 2007; Dieckmann et al. 2008; Fransson et al. 2011; Vancoppenolle et al. 2013) and was estimated to contribute to the total DIC loss of 0.173 mol m^{-2} from the landfast ice from winter to summer. Infiltration of seawater and brine-seawater exchange likely contributed to transient increases in NO$_3$, PO$_4$, and Si(OH)$_4$ in the lower ice prior to biological uptake. Concurrent increases in DIC would be also expected from seawater infiltration,

which would counteract the brine drainage signal and increase the sea-ice DIC inventory, as estimated by increased sea-ice DIC of 0.022 mol m^{-2} through seawater flooding in spring. However, the net effect of seawater infiltration at the ice base was likely minor in the landfast ice based on the seasonal patterns of inorganic nutrient uptake ratios and the low alkalinity, Si(OH)$_4$ and organic matter content in the lower ice relative to higher seawater values. Therefore, brine-seawater exchanges in the landfast ice from winter to summer are considered to be largely controlled by the process of brine rejection (from the ice), rather than seawater infiltration (into the ice), which is further supported by the close behavior of salinity-normalized alkalinity and DIC in the under-ice water and the lower ice, rather than seawater values (discussed below). The process of brine rejection is an important mechanism contributing to the oceanic CO$_2$ sink (Delille et al. 2007; Rysgaard et al. 2007; Vancoppenolle et al. 2013) driven by a seasonal loss of sea-ice DIC in rejected brines, as estimated for Antarctic pack ice (Fransson et al. 2011) and Antarctic landfast sea ice (this study).

The vertical distributions of sea-ice DIC and alkalinity accompanied by elevated Alk : DIC ratios (> 1.8) in the lower 50% of the sea ice, which were higher than those in under-ice water and in surface waters, complemented the mechanism of ikaite precipitation during winter, retention of crystals within the ice and dissolution of ikaite during spring and summer (Rysgaard et al. 2007; Fransson et al. 2011). Ongoing melting of the landfast sea ice would flush any ikaite minerals from the upper and interior ice layers toward the base and/or into the underlying seawater (Rysgaard et al. 2007; Vancoppenolle et al. 2013), resulting in the release of alkalinity in and around the lower ice. Excess alkalinity in the lower ice layers in summer coincided with elevated PO$_4$, POC accumulation, and peak Chl *a* notably at the sea-ice interface. Furthermore, influences of seawater flushing were unlikely to play a major role because the under-ice water during summer had lower PO$_4$ concentrations and lower Alk : DIC ratios (1.13 ± 0.12) relative to the ice at the sea-ice interface. Similar observations of increased alkalinity, attributed to ikaite dissolution in the presence of biofilms, were recently reported in Antarctic landfast sea ice during the summer (van der Linden et al. 2020).

The amount of ikaite precipitated in the landfast sea ice was estimated as 0.066 mol m^{-2} (ΔDIC_{CaCO3}) from relative changes in alkalinity and DIC during the seasonal transitions. Assuming a C : N : P ratio of 106 : 16 : 1 (Redfield et al. 1963), with a mol per mol co-precipitation of PO$_4$ with ikaite and complete dissolution of ikaite and release of PO$_4$ in summer meltwater, approximately 0.62 mmol m^{-2} of PO$_4$ may be liberated during ice melt. Furthermore, PO$_4$ losses of 0.20 and 0.09 mmol m^{-2} are estimated from uptake during primary production and dilution from salinity changes, respectively. For a total winter–summer change in sea-ice PO$_4$ of 0.11 mmol m^{-2}, the residual change of 0.40 mmol m^{-2} is similar to the 0.62 mmol m^{-2} estimated above to be released from

PO$_4$-ikaite interactions during sea-ice melt. These simplistic estimates indicated that there is a net seasonal gain in sea-ice PO$_4$, where CaCO$_3$ (ikaite) processes may play a role in build-up of excess PO$_4$ in the ice. Bacterial assimilation of DIC would also contribute to additional Alk : DIC ratio variability throughout the landfast sea ice but was not assessed in this study (Fransson et al. 2013; Torstensson et al. 2018).

Temporal changes in under-ice water biogeochemistry

Variability of inorganic carbon and nutrients in the under-ice water during the summer (Fig. 5c–h) was likely driven by a combination of meltwater release, mixing of different water masses and biological production of organic matter and biogenic CaCO$_3$ (Henley et al. 2017; Jones et al. 2017; Legge et al. 2017), with further influences on the inorganic carbon cycling from sea-ice ikaite precipitation/dissolution and CO$_2$ exchange. The high inventories of inorganic carbon and nutrients in sea ice that built up during winter are largely retained within the cold and low-porosity ice. The transition to spring and summer and substantial ice-algal primary production led to rapidly reduced DIC and NO$_3$ concentrations and, with a warmed and more porous sea ice, potential for brine and meltwater drainage and sea-ice exchange with the underlying seawater increased. In addition, ikaite processes further reduced sea-ice DIC and alkalinity as values became lower than those in the underlying seawater. However, the distributions of sea-ice inorganic carbon and nutrients indicated minimal effects of seawater flushing and any sea-ice exchange and transfer of the inorganic carbon and nutrient signature from the sea ice would make a transient signal in the under-ice water and subsequently mixed into the comparatively carbon- and nutrient-rich underlying ocean (Henley et al. 2017; Jones et al. 2017; Legge et al. 2017).

Variations in the under-ice water δ^{18}O values (from 1.55‰ to -3.34‰) traced the presence of different water sources during the period of sea-ice melt. Meteoric water is isotopically light, with δ^{18}O for glacial and snow meltwater around -20‰ and -13‰, respectively; distinguished from the isotopically heavier sea-ice meltwater (δ^{18}O ~ 1.8–2.7‰) and CDW (δ^{18}O ~ 0.08‰) (Meredith et al. 2008). Prior to extensive ice melt in summer, values of DIC, alkalinity, NO$_3$ and Si(OH)$_4$ in the under-ice water were similar to those in Ryder Bay (Fig. 5c–g) and typical of this region (Legge et al. 2017; Henley et al. 2019). By early December, increasing contributions of meteoric water were evident as δ^{18}O became isotopically lighter. A transient meteoric signal (-3.34‰) indicated an injection of melted snow, despite co-occurrence of high salinity, which was accompanied by low Alk : DIC ratios that could result from drainage of residual brines where ikaite precipitation (alkalinity depletion) had taken place. In contrast, high Alk : DIC ratios of 1.36 were found in meltwater that contained excess alkalinity relative to depleted CO$_2$ (and DIC) likely due to a combination biological carbon uptake and rejected brine. The temporal changes in δ^{18}O in Ryder Bay

were more subtle ($-1.02‰$ to $-0.54‰$) as the $\delta^{18}O$ signal from snow melt and melting ice is dispersed within the large background of glacial meltwater and CDW (Meredith et al. [2008]).

The landfast ice surface enabled snow to accumulate, which acted as a direct source of isotopically light meltwater to the ice and under-ice water when the ice porosity increased. The patterns in the under-ice water Alk : DIC ratios linked to $\delta^{18}O$ showed that residual brine and meltwater drainage from decaying sea ice strongly influence the underlying seawater during the summer. The freshened under-ice water was nutrient replete, and, with favorable light conditions, rapid DIC and nutrient drawdown occurred. Decreased $Si(OH)_4$ reflected the biological drawdown by pelagic diatoms in the surface water (van Leeuwe et al. [2018], [2020]), possibly with an uptake signal transferred from the sympagic diatom community. Ice algae can act as seed populations to phytoplankton blooms in seasonally ice-covered waters that typically precede pelagic blooms (van Leeuwe et al. [2022]) and drive strong CO_2 uptake in the wake of receding sea ice (Jones et al. [2010]; Riaux-Gobin et al. [2011]; Arrigo et al. [2014]; Jones et al. [2017]).

To investigate the summer dynamics in the under-ice water, two mixing endmember values (source waters) could be considered as (i) Ryder Bay seawater (high S, alkalinity, DIC) and (ii) sea-ice meltwater (low S, alkalinity, DIC) and a theoretical mixing line with Alk_{sal}/DIC_{sal} of 0.8 could be determined (Fig. [6f]). December sea ice yielded a relationship of Alk_{sal}/DIC_{sal} of 1.2 ± 0.1 ($r^2 = 0.87$; $p << 0.001$; $n = 24$) with most points plotting close to the theoretical mixing line. However, different clusters in the Alk_{sal} and DIC_{sal} space could be distinguished. The lower 30% of the ice plotted closer to the Alk_{sal} and DIC_{sal} 2 : 1 trend line with elevated alkalinity relative to DIC (at low Alk_{sal} and DIC_{sal} values) from ice-algal DIC uptake and ikaite dissolution. At higher salinity-normalized alkalinity and DIC_{sal} (2500–4500 μmol kg^{-1}) in the upper ice layers, deviations in the trend were observed with a slope of 1.4 ± 0.2 ($r^2 = 0.94$; $p < 0.01$; $n = 5$). This also indicated excess alkalinity relative to DIC (higher values compared to seawater), which could derive from residual brines trapped in the ice and ikaite crystals that dissolved during analyses. Most under-ice water values plotted along the theoretical mixing line, closer to the seawater endmember value (from parallel sampling in Ryder Bay). Thus, the processes influencing the under-ice water in Hangar Cover were similar to those in Ryder Bay, for example, meltwater inputs, mixing of different water masses, primary production, and calcification (Henley et al. [2017]; Jones et al. [2017]; Legge et al. [2017]), but signals of enhanced biological DIC uptake, brine rejection, and lower alkalinity from biotic and abiotic processes in the sea ice were imprinted on the meltwater-influenced under-ice water. From the end of December, salinity-normalized alkalinity in the under-ice water remained higher than in ice-free surface waters of Ryder Bay, which can be seen as a further indication of a sea-ice source of alkalinity from ikaite processes.

The biogeochemical impact of ikaite processes and sea-ice melt on surface waters and air-sea CO_2 exchange in and around melting landfast sea ice was further investigated by consideration of two different sea-ice ikaite (using Alk : DIC ratios) scenarios (details in "Methods" section). Using a scenario of ikaite precipitation/dissolution (Alk : DIC ~ 1.0) and a scenario of no ikaite precipitation/dissolution (Alk : DIC of 2.3), upon which the sea-ice meltwater is mixed into the summer mixed layer. The two different Alk : DIC ratio scenarios yielded mixed layer pCO_2 values of 148 and 103 μatm, respectively, which are similar to values of surface water pCO_2 of 119 μatm in the vicinity of melting ice in January 2014 in Ryder Bay (Jones et al. [2017]). The difference in pCO_2 of 45 μatm between the low Alk : DIC ratio (no ikaite precipitation/dissolution) and high Alk : DIC ratio (ikaite precipitation/dissolution) scenarios is the driver enhancing the potential for uptake of atmospheric CO_2. These estimates agree well with pCO_2 differences of 56 and 60 μatm determined previously for similar scenarios (Rysgaard et al. [2007]; Fransson et al. [2011]) and highlight the impact of sea-ice ikaite processes and atmospheric CO_2 uptake by a meltwater-influenced ocean. The inorganic carbon dynamics in the landfast sea ice across the seasonal transitions showed that ikaite precipitation in the ice and dissolution in the ice meltwater constituted a minor source of alkalinity to surrounding surface waters. The meltwater released during summer contributed excess alkalinity and an enhanced Alk : DIC ratio to under-ice water, which constituted an important buffer against dilution and enhanced the potential for oceanic CO_2 uptake. This result supports the role of sea-ice carbon dynamics and meltwater-enhanced buffering capacity in coastal waters of the West Antarctic Peninsula as postulated by previous studies in the region (Hauri et al. [2015]; Jones et al. [2017]; Legge et al. [2017]).

Seasonality in biogeochemical cycling in sea ice: Implications for the Antarctic coastal zone

This study indicated that landfast sea ice in this region of the West Antarctic Peninsula was a sink of inorganic carbon of 2.08 g C m^{-2} yr^{-1} from the period of ice formation (May–June) to ice melt (November–December). The net loss of DIC from brine rejection and meltwater dilution was estimated as 0.005 mol m^{-2}, which corresponded to a sink of 0.07 g C m^{-2} yr^{-1} during the full sea-ice cycle. This amount of DIC estimated to be exported within brines was less compared with other Antarctic sea-ice studies (Fransson et al. [2011]), which was likely due to the effect of seawater flooding that resupplied the sea ice with DIC and salt and thus perturbed the magnitude of the brine rejection signal. Biological production of organic matter accounted for depletion of 0.021 to 0.042 mol DIC m^{-2} from winter to summer, with substantial DIC uptake during the winter–spring transition. During the full sea-ice cycle, uptake of 0.50 g C m^{-2} yr^{-1} represented 24% of the total seasonal loss of DIC as a result of ice-algal primary production and associated accumulation of POC and biomass.

Seawater flooding and subsequent seawater-derived DIC, organic matter and salt, could have counteracted the signal of biological DIC uptake in the blooming sympagic algal communities and the effects of brine rejection and meltwater dilution (DIC losses) over the full seasonal cycle.

Formation of ikaite accounted for 0.066 mol m^{-2} of DIC reductions, which was dominated by the removal of 0.061 mol m^{-2} DIC during the spring and summer melt period. The total DIC loss due to incorporation into ikaite corresponded to a decrease in alkalinity of 0.132 mol m^{-2}, that is, 2 : 1 Alk : DIC ratio (Rysgaard et al. 2007; Fransson et al. 2011; Papadimitriou et al. 2012) and yielded an estimate of the amount of ikaite precipitated in the sea ice as 0.066 mol m^{-2}. Release of meltwater reduced alkalinity and DIC through dilution in surface seawater; however, this was slightly counteracted as the sea-ice–derived alkalinity buffered against dilution in the meltwater. Increased sea-ice Alk : DIC ratios from average values of 1.07 ± 0.05 in winter to 1.20 ± 0.26 in spring and 1.50 ± 0.38 in summer, compared with average values of 1.12 ± 0.11 in the under-ice water and 1.09 ± 0.04 in ice-free seawater, revealed fractionation of alkalinity and DIC in the sea ice. During the full sea-ice cycle, this study estimated that seasonal ikaite precipitation removed 0.79 g C m^{-2} yr^{-1}, which represented $\sim 38\%$ of the total seasonal loss of DIC in the landfast sea ice.

The imprint of ice-algal DIC uptake further reduced DIC and increased the potential for atmospheric CO_2 uptake in surface waters. Favorable light conditions, stratification and seeding by ice algae promote phytoplankton blooms and stimulate biological uptake of inorganic carbon in surface waters of the West Antarctic Peninsula (Venables et al. 2013; Jones et al. 2017; van Leeuwe et al. 2022). The presence of sea ice has been shown to promote the development of ice-edge phytoplankton blooms and drawdown of atmospheric CO_2 earlier in the growing season compared to pelagic blooms (Riaux-Gobin et al. 2011; Arrigo et al. 2014; Jones et al. 2015; van Leeuwe et al. 2022). Reduced winter sea-ice cover, deeper mixing and decreased stratification have already been linked to lower phytoplankton biomass and reduced nutrient drawdown in the productive season over the Antarctic shelf (Venables and Meredith 2014; Henley et al. 2017), presumably leading to reductions in biological carbon uptake and a reduced atmospheric CO_2 sink (Legge et al. 2017; Brown et al. 2019).

This study indicated that a scenario of diminishing winter sea ice could also lead to less sea-ice–derived alkalinity released during the melt period. To investigate potential impacts of sea-ice loss and reduced sea-ice alkalinity across the Antarctic landfast sea-ice zone, 18 yr (2000–2018) of circumpolar landfast sea-ice data (Fraser et al. 2020) were used to identify extreme winter (maximum) and summer (minimum) areal extents of the sea ice as 695,159 and 160,217 km^2, respectively. The landfast sea ice analyzed in Hangar Cove during this study and the conceptual model of seasonal sea-ice processes (Fig. 7) were taken to be representative of circum-Antarctic landfast sea ice. Depth-integrated averages of alkalinity over the winter, spring and summer ice cores indicated that 0.132 mol m^{-2} of alkalinity was released from ikaite dissolution in ice meltwater. Therefore, applying the winter (maximum) and summer (minimum) areal coverage as upper and lower bounds, respectively, it was estimated that between 8.2×10^{10} and 2.7×10^{10} mol of alkalinity is potentially released from sea ice across the whole Antarctic landfast ice-sea zone.

As ikaite typically precipitates in first-year sea ice and dissolves in meltwater, the sea-ice carbon (alkalinity) pump is regulated by the cycle of sea ice from formation to melt. Therefore, a reduction in the seasonal sea-ice cover will reduce the impact of the alkalinity pump on inorganic carbon dynamics and air-sea CO_2 exchange in ice-covered seas. If the areal extent of seasonal landfast sea ice around Antarctica declined and only attained a maximum of 160,217 km^2 (i.e., the observed minimum areal extent during 2000–2018; Fraser et al. 2020) as an example of a low-ice scenario, this would potentially correspond to a $\sim 20\%$ reduction in alkalinity released during the seasonal melting of the ice. For a typical meltwater-infused summer surface layer in Ryder Bay (*see* "Temporal changes in under-ice water biogeochemistry" section) and scenario of ikaite precipitation/dissolution (Alk : DIC ratio ~ 2), reductions in sea-ice–derived alkalinity by 20% could lead to increases in surface water pCO_2 by $\sim 400\%$, that is, reaching CO_2 oversaturation of ~ 500 μatm relative to the atmosphere, and a weakening of the oceanic CO_2 sink. Ongoing regional climate change and sea-ice losses are thus expected to decrease the buffering capacity and lower the potential for atmospheric CO_2 uptake in the sea-ice coastal zone of Antarctica.

Conclusion

This multiseasonal study captured significant shifts in carbon and nutrient cycling and sympagic algal communities from winter to summer in landfast sea ice of the West Antarctic Peninsula. This work provided the first time-series measurements of the inorganic carbon system in landfast sea ice, from the period of ice formation to ice melt, in this region. Furthermore, a conceptual model was proposed for processes driving seasonal changes in sea-ice carbon and nutrient patterns during the winter–spring and spring–summer transitions.

The landfast sea ice accumulated substantial amounts of organic matter and algal biomass (approximated by Chl *a* concentrations) in the lower ice layers from winter to summer. Rapid uptake of NO_3 and DIC followed by uptake of $Si(OH)_4$ corresponded to a seasonal succession from heterotrophic to diatom-dominated communities. Concurrent seasonal changes in DIC revealed that the landfast sea ice was a sink for inorganic carbon from the period of ice formation to melt. The overall loss of sea-ice DIC was driven by ice-algal uptake

from winter to spring and abiotic calcium carbonate (ikaite) formation from spring to summer. Physical processes of DIC enrichment from mobility of brines, seawater flooding and dilution from melting ice induced variability in the DIC dynamics in the sea ice.

Winter sea ice enriched with DIC, NO_3, and $Si(OH)_4$ revealed alkalinity and DIC patterns in the upper and interior ice that were indicative of ikaite precipitation. From winter to summer, increasing Alk : DIC ratios indicated that dissolution of ikaite elevated alkalinity in the lower ice and provided a minor source of alkalinity in meltwater released to the underlying seawater. In addition, meltwater inputs transferred the imprint of ice-algal uptake into summer under-ice water in the presence of pelagic phytoplankton uptake, which contributed to large changes in DIC, alkalinity, and nutrients in the under-ice water, relative to ice-free surface waters. These processes showed the influences of sea ice on the upper ocean and enhanced the potential for atmospheric CO_2 drawdown and increased the buffering capacity of seasonally ice-covered waters of coastal Antarctica.

The seasonal patterns of PO_4 were distinctly different compared with those of NO_3 and $Si(OH)_4$. Depleted winter sea-ice PO_4, relative to source seawater, was linked to potential co-precipitation with ikaite. In spring and summer, PO_4 accumulated in the lower ice alongside increasing biomass, which is likely due release upon dissolution of ikaite, preferential remineralization, and accumulation in the presence of biofilms. These results complement those of other studies in Antarctic landfast sea ice with new data of temporal changes in carbon and nutrient cycling from winter to summer in the presence of a seasonal succession of sympagic algae. Furthermore, dynamics in ice-ocean exchanges observed during summer were used to estimate effects of sea-ice–derived alkalinity and implications for atmospheric CO_2 uptake under possible future scenarios of reduced landfast sea ice around Antarctica. This study highlights the need for further investigations into the role of abiotic calcium carbonate (ikaite) processes and interactions with PO_4 and organic matter in Antarctic sea ice.

Data availability statement

All data used in this study can be found in tables in the main text. The carbonate chemistry and inorganic nutrients are available in the Supporting Information Data S1. The inorganic nutrients and organic matter data are stored at https://doi:10.5285/98cc0722-e337-029c-e053-6c86abc02029/ and the pigment data are stored at 10.34894/89N73S. The data used in this study will be available from the British Oceanographic Data Centre upon publication.

References

Arrigo, K., G. Dieckmann, M. Gosselin, D. Robinson, C. Fritsen, and C. Sullivan. 1995. High resolution study of the platelet ice ecosystem in McMurdo Sound, Antarctica: Biomass, nutrient, and production profiles within a dense microalgal bloom. Mar. Ecol. Prog. Ser. **127**: 255–268. doi:10.3354/meps127255

Arrigo, K. R. 2014. Sea ice ecosystems. Ann. Rev. Mar. Sci. **61**: 439–467. doi:10.1146/annurev-marine-010213-135103

Arrigo, K. R., and D. N. Thomas. 2004. Large scale importance of sea ice biology in the Southern Ocean. Antarct. Sci. **164**: 471–486. doi:10.1017/S0954102004002263

Arrigo, K. R., G. van Dijken, and M. Long. 2008. Coastal Southern Ocean: A strong anthropogenic CO_2 sink. Geophys. Res. Lett. **35**: L21602. doi:10.1029/2008gl035624

Arrigo, K. R., Z. W. Brown, and M. M. Mills. 2014. Sea ice algal biomass and physiology in the Amundsen Sea, Antarctica. Elem. Sci. Anthrop. **2**: 000028. doi:10.12952/journal.elementa.000028

Brown, K. A., and others. 2015. Inorganic carbon system dynamics in landfast Arctic sea ice during the early-melt period. J. Geophys. Res. Oceans **120**: 3542–3566. doi:10.1002/2014JC010620

Brown, M. S., D. R. Munro, C. J. Feehan, C. Sweeney, H. W. Ducklow, and O. M. Schofield. 2019. Enhanced oceanic CO_2 uptake along the rapidly changing West Antarctic Peninsula. Nat. Clim. Change **9**: 678–683. doi:10.1038/s41558-019-0552-3

Brzezinski, M. A. 1985. The Si:C:N ratios of marine diatoms: interspecific variability and the effect of some environmental variables. J. Phycol. **21**: 345–357. doi:10.1111/j.0022-3646.1985.00347.x

Clarke, A., M. P. Meredith, M. I. Wallace, M. A. Brandon, and D. N. Thomas. 2008. Seasonal and interannual variability in temperature, chlorophyll and macronutrients in northern Marguerite Bay, Antarctica. Deep. Res. Part II Top. Stud. Oceanogr. **55**: 1988–2006. doi:10.1016/j.dsr2.2008.04.035

Cox, G. F. N., and W. F. Weeks. 1983. Equations for determining the gas and brine volumes in sea ice samples. J. Glaciol. **29**: 306–316. doi:10.3189/S0022143000008364

Cozzi, S. 2008. High-resolution trends of nutrients, DOM and nitrogen uptake in the annual sea ice at Terra Nova Bay, Ross Sea. Ant. Sci. **205**: 441–454. doi:10.1017/S0954102008001247

Delille, B., B. Jourdain, A. V. Borges, J.-L. Tison, and D. Delille. 2007. Biogas CO_2, O_2, dimethylsulfide dynamics in spring Antarctic fast ice. Limnol. Oceanogr. **52**: 1367–1379. doi:10.4319/lo.2007.52.4.1367

Delille, B., and others. 2014. Southern Ocean CO_2 sink: The contribution of sea ice. J. Geophys. Res. Oceans **119**: 6340–6355. doi:10.1002/jgrc.20224

Dickson, A. G. 1981. An exact definition of total alkalinity and a procedure for the estimation of alkalinity and total inorganic carbon from titration data. Deep Sea Res. Part A Oceanogr. Res. Pap. **28**: 609–623. doi:10.1016/0198-01498190121-7

Dickson, A. G., C. Sabine, and J. R. Christian. 2007. Guide to best practices for ocean CO_2 measurements, 3rd ed. PICES Special Publication.

Dieckmann, G. S., and others. 2008. Calcium carbonate as ikaite crystals in Antarctic sea ice. Geophys. Res. Lett. **35**: L08501. doi:10.1029/2008GL033540

Ducklow, H. W., and others. 2007. Marine pelagic ecosystems: The West Antarctic Peninsula. Philos. Trans. R. Soc. B **362**: 67–94. doi:10.1098/rstb.2006.1955

Ducklow, H. W., and others. 2013. West Antarctic Peninsula: An ice-dependent coastal marine ecosystem in transition. Oceanography **26**: 190–203. doi:10.5670/oceanog.2013.62

Fransson, A., M. Chierici, P. L. Yager, and W. O. Smith. 2011. Antarctic sea ice carbon dioxide system and controls. J. Geophys. Res. **116**: C12035. doi:10.1029/2010JC006844

Fransson, A., M. Chierici, L. A. Miller, G. Carnat, H. Thomas, E. Shadwick, S. Pineault, and T. M. Papakyriakou. 2013. Impact of sea ice processes on the carbonate system and ocean acidification state at the ice-water interface of the Amundsen Gulf, Arctic Ocean. J. Geophys. Res. **118**: 1–23. doi:10.1002/2013JC009164

Fraser, A. D., R. A. Massom, K. I. Ohshima, S. Willmes, P. J. Kappes, J. Cartwright, and R. Porter-Smith. 2020. High-resolution mapping of circum-Antarctic landfast sea ice distribution, 2000–2018. Earth Syst. Sci. Data **12**: 2987–2999. doi:10.5194/essd-2020-99

Friis, K., A. Körtzinger, and D. W. R. Wallace. 2003. The salinity normalization of marine inorganic carbon chemistry data. Geophys. Res. Lett. **30**: 1085. doi:10.1029/2002GL015898

Fripiat, F., D. M. Sigman, G. Massé, and J. L. Tison. 2015. High turnover rates indicated by changes in the fixed N forms and their stable isotopes in Antarctic landfast sea ice. J. Geophys. Res. **120**: 3079–3097. doi:10.1002/2014JC010583

Fripiat, F., and others. 2017. Macro-nutrient concentrations in Antarctic pack ice: Overall patterns and overlooked processes. Elem. Sci. Anthrop. **5**: 13. doi:10.1525/elementa.217

Gleitz, M., and D. N. Thomas. 1993. Variation in phytoplankton standing stock, chemical composition and physiology during sea-ice formation in the southeastern Weddell Sea, Antarctica. J. Exp. Mar. Biol. Ecol. **173**: 211–230. doi:10.1016/0022-09819390054-R

Gleitz, M., M. Rutgers van der Loeff, D. N. Thomas, G. S. Dieckmann, and F. J. Millero. 1995. Comparison of summer and winter inorganic carbon, oxygen and nutrient concentrations in Antarctic sea ice brines. Mar. Chem. **51**: 81–91. doi:10.1016/0304-42039500053-T

Golden, K. M., S. F. Ackley, and V. I. Lytle. 1998. The percolation phase transition in sea ice. Science **5397**: 2238–2241. doi:10.1126/science.282.5397.2238

Günther, S., and G. S. Dieckmann. 1999. Seasonal development of algal biomass in snow-covered fast ice and the underlying platelet layer in the Weddell Sea, Antarctica. Antarct. Sci. **11**: 305–315. doi:10.1017/S0954102099000395

Hauri, C., S. C. Doney, T. Takahashi, M. Erickson, G. Jiang, and H. W. Ducklow. 2015. Two decades of inorganic carbon dynamics along the Western Antarctic Peninsula. Biogeosciences **12**: 6761–6779. doi:10.5194/bgd-12-6929-2015

Henley, S. F., and others. 2012. Factors influencing the stable carbon isotopic composition of suspended and sinking organic matter in the coastal Antarctic sea ice environment. Biogeosciences **9**: 1137–1157. doi:10.5194/bg-9-1137-2012

Henley, S. F., R. E. Tuerena, A. L. Annett, A. E. Fallick, M. P. Meredith, H. J. Venables, A. Clarke, and R. S. Ganeshram. 2017. Macronutrient supply, uptake and recycling in the coastal ocean of the west Antarctic Peninsula. Deep Res. Part II Top. Stud. Oceanogr. **139**: 58–76. doi:10.1016/j.dsr2.2016.10.003

Henley, S. F., and others. 2019. Variability and change in the west Antarctic Peninsula marine system: Research priorities and opportunities. Progr. Oceanogr. **173**: 208–237. doi:10.1016/j.pocean.2019.03.003

Hu, Y. B., G. S. Dieckmann, D. A. Wolf-Gladrow, and G. Nehrke. 2014. Laboratory study on coprecipitation of phosphate with ikaite in sea ice. J. Geophys. Res. **119**: 7007–7015. doi:10.1002/2014JC010079

Jeffries, M. O., S. Li, R. A. Jaña, H. R. Krouse, and B. Hurst-Cushing. 1998. Late winter first-year ice floe thickness variability, seawater flooding and snow ice formation in the Amundsen and Ross seas. *In* M. O. Jeffries [ed.], Antarctic sea ice: Physical processes, interactions and variability. Wiley.

Johnson, K. M., J. M. Sieburth, P. J. L. Williams, and L. Brandstrom. 1987. Coulometric total carbon dioxide analysis for marine studies—automation and calibration. Mar. Chem. **21**: 117–133. doi:10.1016/0304-42038790033-8

Jones, E. M., D. C. E. Bakker, H. J. Venables, M. J. Whitehouse, R. E. Korb, and A. J. Watson. 2010. Rapid changes in surface water carbonate chemistry during Antarctic sea ice melt. Tellus B **62**: 621–635. doi:10.1111/j.1600-0889.2010.00496.x

Jones, E. M., D. C. E. Bakker, H. J. Venables, and N. Hardman-Mountford. 2015. Seasonal cycle of CO_2 from the sea ice edge to Island blooms in the Scotia Sea, Southern Ocean. Mar. Chem. **177**: 490–500. doi:10.1016/j.marchem.2015.06.031

Jones, E. M., M. Fenton, M. P. Meredith, N. M. Clargo, S. Ossebaar, H. W. Ducklow, H. J. Venables, and H. J. de Baar. 2017. Ocean acidification and calcium carbonate saturation states in the coastal zone of the West Antarctic Peninsula. Deep Sea Res. Part II Top. Stud. Oceanogr. **139**: 181–194. doi:10.1016/j.dsr2.2017.01.007

Jones, E. P., and A. R. Coote. 1981. Oceanic CO_2 produced by the precipitation of $CaCO_3$ from brines in sea ice. J. Geophy. Res. **86C11**: 11041–11043. doi:10.1029/JC086iC11p11041

Kennedy, H., D. N. Thomas, G. Kattner, C. Haas, and G. S. Dieckmann. 2002. Particulate organic matter in Antarctic

summer sea ice: Concentration and stable isotopic composition. Mar. Ecol. Prog. Ser. **238**: 1–13. doi:10.3354/meps238001

Legendre, L., and others. 1992. Ecology of sea ice biota. Polar Biol. **12**: 429–444. doi:10.1007/BF00243114

Legge, O. J., D. C. E. Bakker, M. T. Johnson, M. P. Meredith, H. J. Venables, P. J. Brown, and G. A. Lee. 2015. The seasonal cycle of ocean-atmosphere CO_2 flux in Ryder Bay, west Antarctic Peninsula. Geophys. Res. Lett. **42**: 2934–2942. doi:10.1002/2015GL063796

Legge, O. J., D. C. E. Bakker, M. Meredith, H. J. Venables, P. J. Brown, E. M. Jones, and M. T. Johnson. 2017. The seasonal cycle of carbonate system processes in Ryder Bay, West Antarctic Peninsula. Deep. Res. Part II Top. Stud. Oceanogr. **39**: 167–180. doi:10.1016/j.dsr2.2016.11.006

Meiners, K., R. Brinkmeyer, M. A. Granskog, and A. Lindfors. 2004. Abundance, size distribution and bacterial colonization of exopolymer particles in Antarctic sea ice Bellingshausen Sea. Aquat. Micro. Ecol. **353**: 283–296. doi:10.3354/ame035283

Meredith, M. P., M. A. Brandon, M. I. Wallace, A. Clarke, M. J. Leng, I. A. Renfrew, N. P. M. van Lipzig, and J. C. King. 2008. Variability in the freshwater balance of northern Marguerite Bay, Antarctic Peninsula: Results from $\delta^{18}O$. Deep. Res. Part II Top. Stud. Oceanogr. **55**: 309–322. doi:10.1016/j.dsr2.2007.11.005

Meredith, M. P., and others. 2017. Changing distributions of sea ice melt and meteoric water west of the Antarctic Peninsula. Deep. Res. Part II Top. Stud. Oceanogr. **139**: 40–57. doi:10.1016/j.dsr2.2016.04.019

Miller, L. A., and others. 2011. Carbon dynamics in sea ice: A winter flux time series. J. Geophys. Res. Oceans **116C2**: C02028. doi:10.1029/2009JC006058

Moreau, S., and others. 2015. Drivers of inorganic carbon dynamics in first-year sea ice: A model study. J. Geophys. Res. Oceans **1201**: 471–495. doi:10.1002/2014JC010388

Murphy, E. J., A. Clarke, C. Symon, and J. Priddle. 1995. Temporal variation in Antarctic sea-ice: Analysis of a long term fast-ice record from the South Orkney Islands. Deep Res. I Oceanogr. Res. Pap. **42**: 1045–1062. doi:10.1016/0967-06379500057-D

Nomura, D., H. Yoshikawa-Inoue, T. Toyota, and K. Shirasawa. 2010. Effects of snow, snow melting and refreezing processes on air-sea-ice CO_2 flux. J. Glaciol. **56196**: 262–270. doi:10.3189/002214310791968548

Papadimitriou, S., H. Kennedy, L. Norman, D. P. Kennedy, G. S. Dieckmann, and D. N. Thomas. 2012. The effect of biological activity, $CaCO_3$ mineral dynamics, and CO_2 degassing in the inorganic carbon cycle in sea ice in late winter-early spring in the Weddell Sea, Antarctica. J. Geophys. Res. **117C8**: C08011. doi:10.1029/2012JC008058

Pedulli, M., J. J. Bisagni, H. W. Ducklow, R. Beardsley, and C. Pilskaln. 2014. Estimates of potential new production PNP

for the waters off the western Antarctic Peninsula WAP region. Cont. Shelf Res. **84**: 54–69. doi:10.1016/j.csr.2014.05.011

Perovich, D. K., B. C. Elder, K. J. Claffey, S. Stammerjohn, R. Smith, S. F. Ackley, H. R. Krousee, and A. J. Gow. 2004. Winter sea-ice properties in Marguerite Bay, Antarctica. Deep Res. II Top. Stud. Oceanogr. **51**: 2023–2039. doi:10.1016/j.dsr2.2004.07.024

Pierrot, D., E. Lewis, and D. W. R. Wallace. 2006. MS Excel program developed for CO_2 system calculations, Rep. ORNL/CDIAC-105a. Carbon Dioxide Information Analysis Center, Oak Ridge National Laboratory, U.S. Department of Energy, Oak Ridge, Tennessee. doi:10.3334/CDIAC/otg.CO2SYS_XLS_CDIAC10

Redfield, A. C., B. H. Ketchum, and F. A. Richards. 1963. The influence of organisms on the composition of seawater, p. 26–77. *In* M. N. Hill [ed.], The sea, v. **2**. John Wiley.

Riaux-Gobin, C., M. Poulin, G. Dieckmann, C. Labrune, and G. Vétion. 2011. Spring phytoplankton onset after the ice break-up and sea-ice signature Adélie Land, East Antarctica. Polar Res. **30**: 5910. doi:10.3402/polar.v30i0.5910

Rysgaard, S., R. N. Glud, M. K. Sejr, J. Bendtsen, and P. B. ChristensenB. 2007. Inorganic carbon transport during sea ice growth and decay: A carbon pump in polar seas. J. Geophys. Res. Oceans **112**: C03016. doi:10.1029/2006JC003572

Saba, G. K., and others. 2014. Winter and spring controls on the summer food web of the coastal West Antarctic Peninsula. Nat. Comm. **51**: 1–8. doi:10.1038/ncomms5318

Saenz, B., and K. R. Arrigo. 2014. Annual primary production in Antarctic sea ice during 2005–2006 from a sea ice state estimate. J. Geophys. Res. **119**: 3645–3678. doi:10.1002/2013JC009677

Schlitzer, R. 2018. Ocean Data View. Available from https://odv.awi.de/

Schofield, O., H. W. Ducklow, D. G. Martinson, M. P. Meredith, M. A. Moline, and W. R. Fraser. 2010. How do polar marine ecosystems respond to rapid climate change? Science **5985**: 1520–1523. doi:10.1126/science.1185779

Smith, W. O., and D. M. Nelson. 1985. Phytoplankton bloom produced by a receding ice edge in the Ross Sea—spatial coherence with the density field. Science **4683**: 163–166. doi:10.1126/science.227.4683.163

Thomas, D. N., and G. S. Dieckmann. 2010. Sea ice, 2nd ed. Wiley-Blackwell.

Torstensson, A., A. Fransson, K. Currie, A. Wulff, and M. Chierici. 2018. Microalgal photophysiology and macronutrient distribution in summer sea ice in the Amundsen and Ross Seas, Antarctica. PLoS One **134**: e0195587. doi:10.1371/journal.pone.0195587

van der Linden, F. C., and others. 2020. Sea ice CO_2 dynamics across seasons: Impact of processes at the interfaces.

J. Geophys. Res. Oceans **125**: e2019JC015807. doi:10.1029/2019JC015807

van Heukelem, L., and C. S. Thomas. 2001. Computer-assisted high-performance liquid chromatography method development with applications to the isolation and analysis of phytoplankton pigments. J. Chromatogr. A **910**: 31–49. doi:10.1016/S0378-43470000603-4

van Leeuwe, M., L. Villerius, J. Roggeveld, R. Visser, and J. Stefels. 2006. An optimized method for automated analysis of algal pigments by HPLC. Mar. Chem. **1023**: 267–275. doi:10.1016/j.marchem.2006.05.003

van Leeuwe, M., and others. 2018. Microalgal community structure and primary production in Arctic and Antarctic sea ice: A synthesis. Elem. Sci. Anthrop. **6**: 4. doi:10.1525/elementa.267

van Leeuwe, M. A., A. L. Webb, H. J. Venables, R. J. Visser, M. P. Meredith, J. T. M. Elzenga, and J. Stefels. 2020. Annual patterns in phytoplankton phenology in Antarctic coastal waters explained by environmental drivers. Limnol. Oceanogr. **9999**: 1–18. doi:10.1002/lno.11477

van Leeuwe, M. A., M. Fenton, E. Davey, J. M. Rintala, E. M. Jones, M. P. Meredith, and J. Stefels. 2022. On the phenology and seeding potential of sea-ice microalgal species. Elem. Sci. Anthrop. **10**: 1. doi:10.1525/elementa.2021.00029

Vancoppenolle, M., and others. 2013. Role of sea ice in global biogeochemical cycles: Emerging views and challenges. Quat. Sci. Rev. **79**: 207–230. doi:10.1016/j.quascirev.2013.04.011

Venables, H. J., A. Clarke, and M. P. Meredith. 2013. Wintertime controls on summer stratification and productivity at the western Antarctic Peninsula. Limnol. Oceanogr. **58**: 1035–1047. doi:10.4319/lo.2013.58.3.1035

Venables, H. J., and M. P. Meredith. 2014. Feedbacks between ice cover, ocean stratification, and heat content in Ryder Bay, West Antarctic Peninsula. J. Geophys. Res. Oceans **119**: 5323–5336. doi:10.1002/jgrc.20224

Vernet, M., D. Martinson, R. Iannuzzi, S. Stammerjohn, W. Kozlowski, K. Sines, R. Smith, and I. Garibotti. 2008. Primary production within the sea-ice zone west of the Antarctic Peninsula: Sea ice, summer mixed layer, and irradiance. Deep Res. II Top. Stud. Oceanogr. **55**: 2068–2085. doi:10.1016/j.dsr2.2008.05.021

Acknowledgments

Conflict of Interest

None declared.